

LAMS-2826

D³-37
C

LAMS-2826

Hydrodynamics

LOS ALAMOS SCIENTIFIC LABORATORY
OF THE UNIVERSITY OF CALIFORNIA • LOS ALAMOS NEW MEXICO

DISTRIBUTION STATEMENT A
Approved for Public Release
Distribution Unlimited

A METHOD FOR EULERIAN FLUID DYNAMICS

LOVELACE FOUNDATION
FOR MEDICAL EDUCATION and RESEARCH
DEPARTMENT OF AEROSPACE MEDICINE
AND BIOASTRONAUTICS

BEST QUALITY INK

Reproduced From
Best Available Copy

20000915 065

3-0

LEGAL NOTICE

This report was prepared as an account of Government sponsored work. Neither the United States, nor the Commission, nor any person acting on behalf of the Commission:

A. Makes any warranty or representation, expressed or implied, with respect to the accuracy, completeness, or usefulness of the information contained in this report, or that the use of any information, apparatus, method, or process disclosed in this report may not infringe privately owned rights; or

B. Assumes any liabilities with respect to the use of, or for damages resulting from the use of any information, apparatus, method, or process disclosed in this report.

As used in the above, "person acting on behalf of the Commission" includes any employee or contractor of the Commission, or employee of such contractor, to the extent that such employee or contractor of the Commission, or employee of such contractor prepares, disseminates, or provides access to, any information pursuant to his employment or contract with the Commission, or his employment with such contractor.

Printed in USA. Price \$ 2.25. Available from the

Office of Technical Services
U. S. Department of Commerce
Washington 25, D. C.

LAMS-2826
UC-32, MATHEMATICS
AND COMPUTERS
TID-4500 (19th Ed.)

LOS ALAMOS SCIENTIFIC LABORATORY
OF THE UNIVERSITY OF CALIFORNIA LOS ALAMOS NEW MEXICO

REPORT WRITTEN: December 1962

REPORT DISTRIBUTED: March 29, 1963

A METHOD FOR EULERIAN FLUID DYNAMICS

by

Marvin Rich

Calculations by

Samuel S. Blackman

Contract W-7405-ENG. 36 with the U. S. Atomic Energy Commission

All LAMS reports are informal documents, usually prepared for a special purpose and primarily prepared for use within the Laboratory rather than for general distribution. This report has not been edited, reviewed, or verified for accuracy. All LAMS reports express the views of the authors as of the time they were written and do not necessarily reflect the opinions of the Los Alamos Scientific Laboratory or the final opinion of the authors on the subject.

ABSTRACT

A method is presented for obtaining numerical solutions of the Eulerian hydrodynamic equations for supersonic compressible flows. The procedure is an adaptation of the PIC method to the case of a continuous fluid. Some discussion is given concerning the limitations of the procedure; the conservation of mass, energy, and momentum; and the treatment of rigid obstacles and two-fluid interfaces. Examples of calculations for flows past a number of cylindrically symmetric objects are also presented.

CONTENTS

	Page
ABSTRACT	3
I. INTRODUCTION	7
II. CALCULATIONAL PROCEDURE	8
A. Description of the Method	8
B. The Difference Equations	11
1. Phase I	11
2. Phase II	13
3. Phase III	15
C. Comments	19
1. Compliance with Conservation Laws	19
2. Stability and Accuracy	24
III. BOUNDARY CONDITIONS AND THE TREATMENT OF SEVERAL FLUIDS	33
A. Boundary Conditions at Open Ends of a Mesh	34
1. Prescribed Input	34
2. Continuous Outflow	34
B. Interactions with Rigid Barriers	35
1. Barriers at Cell Boundaries	35
2. Arbitrary Linear Barriers Within a Cell	37
C. Two Material Cells	42
IV. CALCULATIONS OF SUPERSONIC FLOW PAST BLUNT CYLINDRICAL OBSTACLES	53
REFERENCES	83
APPENDIX I	84
APPENDIX II	87
APPENDIX III	91

I. INTRODUCTION

This report has been written with a two-fold purpose. The first is to record a set of procedures developed several years ago for the numerical solution of the Eulerian hydrodynamic equations for compressible isentropic flow. The second is to present the results of some recent computations on the supersonic flow of air past a variety of cylindrically symmetric objects.

The procedure for solving the hydrodynamic equations to be described here is closely related to the semi-Eulerian "Particle-in-Cell" (PIC) method¹ and is in fact merely an extension of that approach to a continuous fluid. Like the PIC method, it is applicable to a wide variety of multi-fluid hydrodynamic problems in one or more dimensions and is particularly suited to situations involving large distortions of the fluid. Limitations of the procedure are imposed primarily by bounded instabilities which arise when large portions of the fluid under consideration move at velocities below the local sound speeds. Otherwise, calculational accuracy is governed mainly by the fineness of the Eulerian difference mesh one must use, which is determined by the storage capacity and speed of available digital computers.

Sections II and III of this report are devoted to a discussion of the numerical techniques involved in the solution of the hydrodynamic equations. In Section IV, theoretical results are given for steady-state flow around right circular cylinders with conical noses of various apex angles and at various Mach numbers between one and five. Comparisons of the computed positions of detached shocks and of the pressure distribution about the obstacle nose are made with the experimental results of Marschner² and Oguchi.³

II. CALCULATIONAL PROCEDURE

A. Description of the Method

The method for solving the hydrodynamic equations which is described below finds its primary applications in two-dimensional problems. We will therefore forego a discussion of the procedure in one dimension and begin immediately with a discussion of the two-dimensional differencing scheme. For simplicity, only a single fluid in Cartesian coordinates will be considered at this time.

In order to obtain a system of difference equations to describe the motion of the fluid, we assume that the region of fluid under consideration is covered by a fixed (Eulerian) grid of rectangular cells of sides Δx and Δy (Fig. 1).

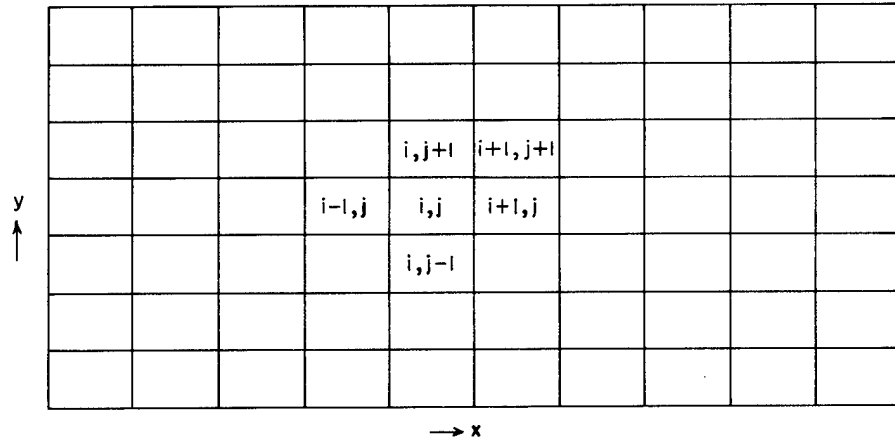


Figure 1. Example of a two dimensional Eulerian mesh

Each cell is labeled by the pair of integers (i,j) which denote the location of the cell center with respect to some origin. Half integer indices are used to denote cell boundaries. For example, the indices $(i+\frac{1}{2},j)$ refer to the right-hand boundary of cell (i,j) , and $(i,j-\frac{1}{2})$ refers to the lower boundary of this cell. A calculation is begun by assigning values for the density ρ , velocity \vec{v} , and specific energy E of the fluid at the center of each cell at the initial time $t = 0$. From these initial conditions the configuration of the fluid over the mesh is obtained at a slightly later time $t = \Delta t$ by means of the hydrodynamic equations of motion. In general, one proceeds cyclically to calculate the state of the fluid at time $t = n\Delta t$ from the state at time $t = (n-1)\Delta t$ where n is an integer which will henceforth be used without the Δt to denote the time.

In integral form, the hydrodynamic equations for compressible isentropic flow are

$$\int_{V(t)} \frac{\partial \rho}{\partial t} d\tau = - \int_{S(t)} \rho \vec{v} \cdot d\vec{s} \quad (1)$$

$$\frac{\partial}{\partial t} \int_{V(t)} \rho \vec{v} d\tau = - \int_{S(t)} p d\vec{s} \quad (2)$$

$$\frac{\partial}{\partial t} \int_{V(t)} E d\tau = - \int_{S(t)} p \vec{v} \cdot d\vec{s} \quad (3)$$

$$p = p(\rho, I) \quad (4)$$

Here, we are considering integration over a specific element of fluid occupying volume $V(t)$ at time t and bounded by surface $S(t)$. It is assumed that no external forces or internal dissipative mechanisms are present and that the motion of an element of fluid is produced solely by the pressure p exerted on this volume by neighboring fluid elements. The first three equations are statements of the conservation of mass, momentum, and energy of the fluid; and the last, the equation of state, relates the pressure of the fluid to the density and the specific internal energy, $I = E - \frac{1}{2} \vec{v}^2$.

In differencing these equations, we will consider the volume $V(t)$ to be that of some arbitrary cell (i,j) and the surface $S(t)$ to represent the four sides of this cell.

As in the PIC method,¹ the calculation of the time $(n+1)$ configuration of the fluid from that at time n may be thought of as proceeding in three steps. In the first, the fluid element in each cell is assumed fixed and no flow across the cell boundaries is allowed. By applying Eqs. (2), (3), and (4), intermediate values of the velocity and specific energy in each cell are obtained. The second phase consists of the calculation of the mass flows across the cell boundaries.

Mass crossing a boundary is assumed to carry with it the intermediate velocity and specific energy of the cell from which it came. In the third phase, the new cell densities are computed; and by application of conservation of energy and momentum, the new velocities and specific energies are subsequently obtained.

In the following, all cells under consideration will be assumed interior to the fluid. The effect of boundaries will be left for later discussion.

B. The Difference Equations

1. Phase I

It is assumed that the following quantities are known at the center of each cell (i,j) at time n , i.e., $t = n\Delta t$, and that for purposes of differencing they remain constant throughout the cell:

$$\begin{aligned} \text{density:} & \quad \rho_{i,j}^{(n)} \\ \text{velocity:} & \quad u_{i,j}^{(n)} \quad (\text{x component}) \\ & \quad v_{i,j}^{(n)} \quad (\text{y component}) \\ \text{specific energy:} & \quad E_{i,j}^{(n)} \end{aligned}$$

By applying the equation of state Eq. (4), the pressure at the center of each cell is obtained,

$$p_{i,j}^{(n)} = p \left\{ \rho_{i,j}^{(n)}, E_{i,j}^{(n)} - \frac{1}{2} \left[u_{i,j}^{(n)^2} + v_{i,j}^{(n)^2} \right] \right\}$$

Integrating Eqs. (2) and (3) over the volume of cell (i,j) at time n results in the difference equations,

$$\rho_{i,j}^{(n)} \left(\frac{\partial u}{\partial t} \right)_{i,j}^{(n)} \Delta x \Delta y = - \left[p_{i+\frac{1}{2},j}^{(n)} - p_{i-\frac{1}{2},j}^{(n)} \right] \Delta y$$

$$\rho_{i,j}^{(n)} \left(\frac{\partial v}{\partial t} \right)_{i,j}^{(n)} \Delta x \Delta y = - \left[p_{i,j+\frac{1}{2}}^{(n)} - p_{i,j-\frac{1}{2}}^{(n)} \right] \Delta x$$

$$\begin{aligned} \rho_{i,j}^{(n)} \left(\frac{\partial E}{\partial t} \right)_{i,j}^{(n)} \Delta x \Delta y = & - \left\{ \left[p_{i+\frac{1}{2},j}^{(n)} u_{i+\frac{1}{2},j}^{(n)} - p_{i-\frac{1}{2},j}^{(n)} u_{i-\frac{1}{2},j}^{(n)} \right] \Delta y \right. \\ & \left. + \left[p_{i,j+\frac{1}{2}}^{(n)} v_{i,j+\frac{1}{2}}^{(n)} - p_{i,j-\frac{1}{2}}^{(n)} v_{i,j-\frac{1}{2}}^{(n)} \right] \Delta x \right\} \end{aligned}$$

The assumption of no mass flow has been used to remove the density from the time derivative on the left-hand sides of these equations. The pressures and velocities on the right refer to the cell boundaries and are taken as simple averages of these quantities in the cells separated by a given boundary. For instance,

$$p_{i+\frac{1}{2},j}^{(n)} = \frac{1}{2} \left[p_{i,j}^{(n)} + p_{i+1,j}^{(n)} \right]$$

Defining the time derivatives on the left sides of these equations by

$$\left(\frac{\partial u}{\partial t} \right)_{i,j}^{(n)} = \frac{\tilde{u}_{i,j}^{(n)} - u_{i,j}^{(n)}}{\Delta t}$$

$$\left(\frac{\partial v}{\partial t} \right)_{i,j}^{(n)} = \frac{\tilde{v}_{i,j}^{(n)} - v_{i,j}^{(n)}}{\Delta t}$$

$$\left(\frac{\partial E}{\partial t}\right)_{i,j}^{(n)} = \frac{\tilde{E}_{i,j}^{(n)} - E_{i,j}^{(n)}}{\Delta t}$$

we arrive at the following equations for the intermediate velocity and specific energy, which are distinguished by a tilde symbol:

$$\tilde{u}_{i,j}^{(n)} = u_{i,j}^{(n)} - \frac{p_{i+\frac{1}{2},j}^{(n)} - p_{i-\frac{1}{2},j}^{(n)}}{\Delta x} \frac{\Delta t}{\rho_{i,j}^{(n)}} \quad (5)$$

$$\tilde{v}_{i,j}^{(n)} = v_{i,j}^{(n)} - \frac{p_{i,j+\frac{1}{2}}^{(n)} - p_{i,j-\frac{1}{2}}^{(n)}}{\Delta y} \frac{\Delta t}{\rho_{i,j}^{(n)}} \quad (6)$$

$$\begin{aligned} \tilde{E}_{i,j}^{(n)} = E_{i,j}^{(n)} - & \left[\frac{p_{i+\frac{1}{2},j}^{(n)} u_{i+\frac{1}{2},j}^{(n)} - p_{i-\frac{1}{2},j}^{(n)} u_{i-\frac{1}{2},j}^{(n)}}{\Delta x} \right. \\ & \left. + \frac{p_{i,j+\frac{1}{2}}^{(n)} v_{i,j+\frac{1}{2}}^{(n)} - p_{i,j-\frac{1}{2}}^{(n)} v_{i,j-\frac{1}{2}}^{(n)}}{\Delta y} \right] \frac{\Delta t}{\rho_{i,j}^{(n)}} \quad (7) \end{aligned}$$

2. Phase II

From the right-hand side of Eq. (1) it is seen that the flow across a boundary from one cell into another is proportional to the fluid density and normal component of velocity at the interface. Equation (1) differences into the following equation expressing the conservation of mass:

$$\rho_{i,j}^{(n+1)} \Delta x \Delta y = \rho_{i,j}^{(n)} \Delta x \Delta y - \Delta M_{i+\frac{1}{2},j}^{(n)} + \Delta M_{i-\frac{1}{2},j}^{(n)} - \Delta M_{i,j+\frac{1}{2}}^{(n)} + \Delta M_{i,j-\frac{1}{2}}^{(n)} \quad (8)$$

where

$$\Delta M_{i+\frac{1}{2},j}^{(n)} = \rho_{i+\frac{1}{2},j}^{(n)} \tilde{u}_{i+\frac{1}{2},j}^{(n)} \Delta y \Delta t \quad (9)$$

$$\Delta M_{i,j+\frac{1}{2}}^{(n)} = \rho_{i,j+\frac{1}{2}}^{(n)} \tilde{v}_{i,j+\frac{1}{2}}^{(n)} \Delta x \Delta t$$

etc. are the mass flows across the cell boundaries indicated by the subscripts.

It has been found that it is now no longer adequate to use simple averages for the densities and velocities at the cell boundaries as was done in Phase I. Doing so tends to lead to minor but noticeable instabilities in the solution of the difference equations. Instead, a weighting must be given these quantities in preference of the cell out of which the fluid flows. (This necessity arises "naturally" when one remembers that due to the finite time step, Δt , the center of the fluid element leaving a cell lies somewhat within the cell and not at the boundary.) In the mass flow calculation, the boundary quantities can be obtained from the first two terms of a Taylor expansion about the center of the emptying cell. Thus the equations for the boundary quantities depend on the direction of flow at the cell interface. For the right-hand boundary of cell (i,j) , for instance, the mass flow $\Delta M_{i+\frac{1}{2},j}^{(n)}$ would be calculated as follows:

If $\tilde{u}_{i,j}^{(n)} + \tilde{u}_{i+1,j}^{(n)} > 0$ and

$$\tilde{u}_{i+\frac{1}{2},j}^{(n)} \equiv \tilde{u}_{i,j}^{(n)} + \left(\frac{\partial \tilde{u}}{\partial x}\right)_{i,j}^{(n)} \frac{\Delta x}{2} = \tilde{u}_{i,j}^{(n)} + \frac{\tilde{u}_{i+1,j}^{(n)} - \tilde{u}_{i-1,j}^{(n)}}{4} > 0$$

then

$$\Delta M_{i+\frac{1}{2},j}^{(n)} = \left[\tilde{u}_{i,j}^{(n)} + \frac{\tilde{u}_{i+1,j}^{(n)} - \tilde{u}_{i-1,j}^{(n)}}{4} \right] \left[\rho_{i,j}^{(n)} + \frac{\rho_{i+1,j}^{(n)} - \rho_{i-1,j}^{(n)}}{4} \right] \Delta y \Delta t$$

If $\tilde{u}_{i,j}^{(n)} + \tilde{u}_{i+1,j}^{(n)} < 0$ and

$$\tilde{u}_{i+\frac{1}{2},j}^{(n)} \equiv \tilde{u}_{i+1,j}^{(n)} - \left(\frac{\partial \tilde{u}}{\partial x} \right)_{i+1,j}^{(n)} \frac{\Delta x}{2} = \tilde{u}_{i+1,j}^{(n)} - \frac{\tilde{u}_{i+2,j}^{(n)} - \tilde{u}_{i,j}^{(n)}}{4} < 0$$

then

$$\Delta M_{i+\frac{1}{2},j}^{(n)} = \left[\tilde{u}_{i+1,j}^{(n)} - \frac{\tilde{u}_{i+2,j}^{(n)} - \tilde{u}_{i,j}^{(n)}}{4} \right] \left[\rho_{i+1,j}^{(n)} - \frac{\rho_{i+2,j}^{(n)} - \rho_{i,j}^{(n)}}{4} \right] \Delta y \Delta t$$

Otherwise $\Delta M_{i+\frac{1}{2},j}^{(n)} = 0$.

The flows across the other three sides of cell (i,j) are obtained in a similar manner. The requirement that the sign of the simple average boundary velocity $\left[\tilde{u}_{i,j}^{(n)} + \tilde{u}_{i+1,j}^{(n)} \right]$, in the case above be used in determining the form for the mass flow term ensures that a calculation will be independent of the direction one chooses in progressing from cell to cell through the mesh.

When more than one fluid is present it is convenient to drop the derivative part of the density term in the above mass flow equation, leaving only the first term in the Taylor expansion. This does not noticeably affect the stability of the difference equations.

3. Phase III

Mass flowing from one cell to another is assumed to carry with it the tilde velocity and specific energy of the cell from which it came. Thus, after the mass flow, the composition of a given cell may be thought of as

having a fraction with mass M_1 at velocity \vec{v}_1 and specific energy E_1 , a portion M_2 with velocity \vec{v}_2 and specific energy E_2 , etc. A single velocity and specific energy for the cell can be obtained by applying the laws of conservation of momentum and energy:

$$\vec{v}_{\text{final}} = \frac{\sum_k M_k \vec{v}_k}{\sum_k M_k}$$

$$E_{\text{final}} = \frac{\sum_k M_k E_k}{\sum_k M_k}$$

To illustrate this by a specific example, consider the changes in cell (i,j) due to the transport of fluid. We assume that the fluid flow in the neighborhood of this cell is upward and to the right. Therefore, fluid flows into (i,j) across its lower and left boundaries and flows out across its upper and right-hand sides. The composition of the cell after transport is as follows:

mass:

$$M_1 \equiv \Delta M_{i-\frac{1}{2},j}^{(n)}$$

$$M_2 \equiv \Delta M_{i,j-\frac{1}{2}}^{(n)}$$

$$M_3 \equiv \left[\rho_{i,j}^{(n)} \Delta x \Delta y - \Delta M_{i+\frac{1}{2},j}^{(n)} - \Delta M_{i,j+\frac{1}{2}}^{(n)} \right]$$

carrying velocity:

$$\left[\tilde{u}_{i-1,j}^{(n)}, \tilde{v}_{i-1,j}^{(n)} \right]$$

$$\left[\tilde{u}_{i,j-1}^{(n)}, \tilde{v}_{i,j-1}^{(n)} \right]$$

$$\left[\tilde{u}_{i,j}^{(n)}, \tilde{v}_{i,j}^{(n)} \right]$$

carrying specific energy:

$$\tilde{E}_{i-1,j}^{(n)}$$

$$\tilde{E}_{i,j-1}^{(n)}$$

$$\tilde{E}_{i,j}^{(n)}$$

The time $(n+1)$ parameters for cell (i,j) will thus be

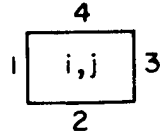
$$\rho_{i,j}^{(n+1)} = \frac{M_1 + M_2 + M_3}{\Delta x \Delta y}$$

$$u_{i,j}^{(n+1)} = \frac{M_1 \tilde{u}_{i-1,j}^{(n)} + M_2 \tilde{u}_{i,j-1}^{(n)} + M_3 \tilde{u}_{i,j}^{(n)}}{\rho_{i,j}^{(n+1)} \Delta x \Delta y}$$

$$v_{i,j}^{(n+1)} = \frac{M_1 \tilde{v}_{i-1,j}^{(n)} + M_2 \tilde{v}_{i,j-1}^{(n)} + M_3 \tilde{v}_{i,j}^{(n)}}{\rho_{i,j}^{(n+1)} \Delta x \Delta y}$$

$$E_{i,j}^{(n+1)} = \frac{M_1 \tilde{E}_{i-1,j}^{(n)} + M_2 \tilde{E}_{i,j-1}^{(n)} + M_3 \tilde{E}_{i,j}^{(n)}}{\rho_{i,j}^{(n+1)} \Delta x \Delta y}$$

More generally, if the four sides of cell (i,j) are numbered by k = 1, 2, 3, and 4 as shown below,



we can define a function $C_{i,j}(k)$ for this cell referring to side k such that

$$\begin{aligned} C_{i,j}(k) &= 1 \text{ if fluid flows into cell (i,j) across side } k \\ &= 0 \text{ if fluid flows out of cell (i,j) across side } k \end{aligned}$$

Then the final velocity and energy are given by the expressions

$$\begin{aligned} u_{i,j}^{(n+1)} &= \left(C_{i,j}(1) \tilde{u}_{i-1,j}^{(n)} \Delta M_{i-\frac{1}{2},j}^{(n)} + C_{i,j}(2) \tilde{u}_{i,j-1}^{(n)} \Delta M_{i,j-\frac{1}{2}}^{(n)} \right. \\ &\quad \left. + C_{i,j}(3) \tilde{u}_{i+1,j}^{(n)} \Delta M_{i+\frac{1}{2},j}^{(n)} \right. \\ &\quad \left. + C_{i,j}(4) \tilde{u}_{i,j+1}^{(n)} \Delta M_{i,j+\frac{1}{2}}^{(n)} + \tilde{u}_{i,j}^{(n)} \left\{ \rho_{i,j}^{(n)} \Delta x \Delta y - [1 - C_{i,j}(1)] \right. \right. \\ &\quad \left. \times \Delta M_{i-\frac{1}{2},j}^{(n)} - [1 - C_{i,j}(2)] \Delta M_{i,j-\frac{1}{2}}^{(n)} \right. \\ &\quad \left. \left. - [1 - C_{i,j}(3)] \Delta M_{i+\frac{1}{2},j}^{(n)} - [1 - C_{i,j}(4)] \Delta M_{i,j+\frac{1}{2}}^{(n)} \right\} \right) / \left[\rho_{i,j}^{(n+1)} \Delta x \Delta y \right] \quad (10) \end{aligned}$$

$$\begin{aligned} v_{i,j}^{(n+1)} &= \left(C_{i,j}(1) \tilde{v}_{i-1,j}^{(n)} \Delta M_{i-\frac{1}{2},j}^{(n)} + C_{i,j}(2) \tilde{v}_{i,j-1}^{(n)} \Delta M_{i,j-\frac{1}{2}}^{(n)} \right. \\ &\quad \left. + C_{i,j}(3) \tilde{v}_{i+1,j}^{(n)} \Delta M_{i+\frac{1}{2},j}^{(n)} + \right. \quad (11) \end{aligned}$$

(Equation continued)

$$\begin{aligned}
& + C_{i,j}^{(4)} \tilde{v}_{i,j+1}^{(n)} \Delta M_{i,j+\frac{1}{2}}^{(n)} + \tilde{v}_{i,j}^{(n)} \left\{ \rho_{i,j}^{(n)} \Delta x \Delta y - [1 - C_{i,j}^{(1)}] \right. \\
& \quad \times \Delta M_{i-\frac{1}{2},j}^{(n)} - [1 - C_{i,j}^{(2)}] \Delta M_{i,j-\frac{1}{2}}^{(n)} \\
& \quad \left. - [1 - C_{i,j}^{(3)}] \Delta M_{i+\frac{1}{2},j}^{(n)} - [1 - C_{i,j}^{(4)}] \Delta M_{i,j+\frac{1}{2}}^{(n)} \right\} \Big/ \left[\rho_{i,j}^{(n+1)} \Delta x \Delta y \right] \\
E_{i,j}^{(n+1)} = & \left(C_{i,j}^{(1)} \tilde{E}_{i-1,j} \Delta M_{i-\frac{1}{2},j}^{(n)} + C_{i,j}^{(2)} \tilde{E}_{i,j-1} \Delta M_{i,j-\frac{1}{2}}^{(n)} \right. \\
& + C_{i,j}^{(3)} \tilde{E}_{i+1,j} \Delta M_{i+\frac{1}{2},j}^{(n)} \\
& + C_{i,j}^{(4)} \tilde{E}_{i,j+1} \Delta M_{i,j+\frac{1}{2}}^{(n)} + \tilde{E}_{i,j}^{(n)} \left\{ \rho_{i,j}^{(n)} \Delta x \Delta y - [1 - C_{i,j}^{(1)}] \right. \\
& \quad \times \Delta M_{i-\frac{1}{2},j}^{(n)} - [1 - C_{i,j}^{(2)}] \Delta M_{i,j-\frac{1}{2}}^{(n)} \\
& \quad \left. - [1 - C_{i,j}^{(3)}] \Delta M_{i+\frac{1}{2},j}^{(n)} - [1 - C_{i,j}^{(4)}] \Delta M_{i,j+\frac{1}{2}}^{(n)} \right\} \Big/ \left[\rho_{i,j}^{(n+1)} \Delta x \Delta y \right] \quad (12)
\end{aligned}$$

This completes the transition of the fluid configuration from time n to time $(n+1)$.

C. Comments

In this section a discussion will be given of such questions as the conservation of mass, energy, and momentum within the framework of the difference equations, and the stability and accuracy of the method.

1. Compliance with Conservation Laws

Consider a rectangular array of cells covering a region of fluid

under investigation and labeled by cell indices extending from $i = 1$ to $i = i_{\max}$ and $j = 1$ to $j = j_{\max}$. We want to examine the change of the total mass, energy, and momentum within the mesh between time $n\Delta t$ and $(n+1)\Delta t$. In particular, we want to show that the differencing scheme described above is consistent with the conservation of mass, energy, and momentum.

a. Mass Conservation

The change in the mass of cell (i,j) in the transition from time $n\Delta t$ to $(n+1)\Delta t$ is

$$\Delta M_{i,j}^{(n)} \equiv \left[\rho_{i,j}^{(n+1)} - \rho_{i,j}^{(n)} \right] \Delta x \Delta y = \Delta M_{i-\frac{1}{2},j}^{(n)} - \Delta M_{i+\frac{1}{2},j}^{(n)} + \Delta M_{i,j-\frac{1}{2}}^{(n)} - \Delta M_{i,j+\frac{1}{2}}^{(n)}$$

The mass change for the entire system in this time interval is therefore

$$\begin{aligned} \Delta M^{(n)} &= \sum_{i=1}^{i_{\max}} \sum_{j=1}^{j_{\max}} \Delta M_{i,j}^{(n)} \\ &= \sum_{i,j} \left[\Delta M_{i-\frac{1}{2},j}^{(n)} - \Delta M_{i+\frac{1}{2},j}^{(n)} + \Delta M_{i,j-\frac{1}{2}}^{(n)} - \Delta M_{i,j+\frac{1}{2}}^{(n)} \right] \end{aligned}$$

Since the mass flow into cell (i,j) from the left is equal to the flow out of cell $(i-1,j)$ from the right, etc., all terms in this sum pertaining to boundaries interior to the mesh cancel one another leaving the result

$$\Delta M^{(n)} = \sum_{j=1}^{j_{\max}} \left[\Delta M_{\frac{1}{2},j}^{(n)} - \Delta M_{i_{\max}+\frac{1}{2},j}^{(n)} \right] + \sum_{i=1}^{i_{\max}} \left[\Delta M_{i,\frac{1}{2}}^{(n)} - \Delta M_{i,j_{\max}+\frac{1}{2}}^{(n)} \right]$$

The mass change of the system in the course of one calculation cycle is seen to be due to fluid entering or leaving across the limiting boundaries

of the mesh. No "creation" or "destruction" of mass occurs in the interior of the mesh.

b. Energy and Momentum Conservation

The redistribution of energy and momentum among the mesh cells occurs in two separate ways within a calculation cycle: first in Phase I, where each cell is treated as a Lagrangian mass element and fluid is restrained from flowing, and again in Phase III, where the effects of the mass transport are taken into account.

In Phase I, energy and momentum are transmitted to a cell by means of the pressure forces acting upon it. The change in these quantities within the system is the difference between the sum of the tilde and the initial energy and momenta of the mesh cells.

$$\Delta \tilde{E}_T = \sum_{i=1}^{i_{\max}} \sum_{j=1}^{j_{\max}} \rho_{i,j}^{(n)} \left[\tilde{E}_{i,j}^{(n)} - E_{i,j}^{(n)} \right] \Delta x \Delta y$$

$$\Delta \vec{P}_T = \sum_{i=1}^{i_{\max}} \sum_{j=1}^{j_{\max}} \rho_{i,j}^{(n)} \left[\vec{\tilde{v}}_{i,j}^{(n)} - \vec{v}_{i,j}^{(n)} \right] \Delta x \Delta y$$

Inserting the expressions for $\vec{v}_{i,j}^{(n)}$ and $\tilde{E}_{i,j}^{(n)}$ [Eqs. (5, 6, 7)] into these equations gives

$$\Delta \tilde{E}_T = - \sum_{i,j} \Delta x \Delta y \left[\frac{p_{i+\frac{1}{2},j}^{(n)} u_{i+\frac{1}{2},j}^{(n)} - p_{i-\frac{1}{2},j}^{(n)} u_{i-\frac{1}{2},j}^{(n)}}{\Delta x} \right. \\ \left. + \frac{p_{i,j+\frac{1}{2}}^{(n)} v_{i,j+\frac{1}{2}}^{(n)} - p_{i,j-\frac{1}{2}}^{(n)} v_{i,j-\frac{1}{2}}^{(n)}}{\Delta y} \right] \Delta t$$

$$\Delta \tilde{P}_{T,x} = - \sum_{i,j} \Delta x \Delta y \frac{p_{i+\frac{1}{2},j}^{(n)} - p_{i-\frac{1}{2},j}^{(n)}}{\Delta x} \Delta t$$

$$\Delta \tilde{P}_{T,y} = - \sum_{i,j} \Delta x \Delta y \frac{p_{i,j+\frac{1}{2}}^{(n)} - p_{i,j-\frac{1}{2}}^{(n)}}{\Delta y} \Delta t$$

As in the case of the mass flow, all terms pertaining to cell boundaries interior to the mesh appear twice — once with a positive and once with a negative sign, and so cancel. We are left with energy and momentum flux terms between the boundary of the mesh and the exterior region only

$$\begin{aligned} \Delta \tilde{E} &= \sum_{j=1}^{j_{\max}} \left[p_{\frac{1}{2},j}^{(n)} u_{\frac{1}{2},j}^{(n)} - p_{i_{\max}+\frac{1}{2},j}^{(n)} u_{i_{\max}+\frac{1}{2},j}^{(n)} \right] \Delta y \Delta t \\ &\quad + \sum_{i=1}^{i_{\max}} \left[p_{i,\frac{1}{2}}^{(n)} v_{i,\frac{1}{2}}^{(n)} - p_{i,j_{\max}+\frac{1}{2}}^{(n)} v_{i,j_{\max}+\frac{1}{2}}^{(n)} \right] \Delta x \Delta t \\ \Delta \tilde{P}_x &= \sum_{j=1}^{j_{\max}} \left[p_{\frac{1}{2},j}^{(n)} - p_{i_{\max}+\frac{1}{2},j}^{(n)} \right] \Delta y \Delta t \\ \Delta \tilde{P}_y &= \sum_{i=1}^{i_{\max}} \left[p_{i,\frac{1}{2}}^{(n)} - p_{i,j_{\max}+\frac{1}{2}}^{(n)} \right] \Delta x \Delta t \end{aligned}$$

Similarly, in Phase III mass crossing a cell boundary carries with it an amount of energy and momentum determined by the specific energy and velocity of the cell from which it is removed. As was mentioned in the discussion of this phase of the calculation cycle, conservation of energy

and momentum are used explicitly to ensure that energy and momentum lost by one cell are gained by another. (The equations that demonstrate this are identical to those illustrating mass conservation except that now the mass flows would be multiplied by appropriate specific energy or velocity components.) The energy and momentum changes of the system occurring in Phase III are

$$\begin{aligned}
 \Delta E^{III} &= \sum_{i=1}^{i_{\max}} \left[\Delta M_{i,\frac{1}{2}}^{(n)} \tilde{E}_{i,L}^{(n)} - \Delta M_{i,j_{\max}+\frac{1}{2}}^{(n)} \tilde{E}_{i,U}^{(n)} \right] \\
 &+ \sum_{j=1}^{j_{\max}} \left[\Delta M_{\frac{1}{2},j}^{(n)} \tilde{E}_{L,j}^{(n)} - \Delta M_{i_{\max}+\frac{1}{2},j}^{(n)} \tilde{E}_{R,j}^{(n)} \right] \\
 \Delta P_x^{III} &= \sum_{i=1}^{i_{\max}} \left[\Delta M_{i,\frac{1}{2}}^{(n)} \tilde{u}_{i,L}^{(n)} - \Delta M_{i,j_{\max}+\frac{1}{2}}^{(n)} \tilde{u}_{i,U}^{(n)} \right] \\
 &+ \sum_{j=1}^{j_{\max}} \left[\Delta M_{\frac{1}{2},j}^{(n)} \tilde{u}_{L,j}^{(n)} - \Delta M_{i_{\max}+\frac{1}{2},j}^{(n)} \tilde{u}_{R,j}^{(n)} \right] \\
 \Delta P_y^{III} &= \sum_{i=1}^{i_{\max}} \left[\Delta M_{i,\frac{1}{2}}^{(n)} \tilde{v}_{i,L}^{(n)} - \Delta M_{i,j_{\max}+\frac{1}{2}}^{(n)} \tilde{v}_{i,U}^{(n)} \right] \\
 &+ \sum_{j=1}^{j_{\max}} \left[\Delta M_{\frac{1}{2},j}^{(n)} \tilde{v}_{L,j}^{(n)} - \Delta M_{i_{\max}+\frac{1}{2},j}^{(n)} \tilde{v}_{R,j}^{(n)} \right]
 \end{aligned}$$

where $\tilde{E}_{i,L}^{(n)}$ is the tilde specific energy of the cell in column i on

the lower boundary of the mesh from which the mass is flowing, and similarly for the other energy and velocity terms. If mass is flowing into the system from outside the mesh, the energies and velocities to be used are specified by the external conditions imposed on the calculation.

The total energy and momentum changes per cycle are the sums of the contributions to these quantities from Phases I and III. Energy and momentum are rigorously conserved within the differencing scheme and their changes can occur only through interaction with the region exterior to the mesh.

2. Stability and Accuracy

No thorough analysis of the questions of the stability and accuracy of the difference scheme described above has been made. The following comments will therefore either be of a self-evident nature or will be based largely on observations on past calculational experiments.

Stability and accuracy are closely related. Both can be affected by relatively small changes in the higher order derivative terms implied by the replacement of the differential hydrodynamic equations by difference equations. Basically, the difference scheme under consideration is accurate to first order in the time and space intervals. However true accuracy at the end of an extended calculation depends not only on the accuracy over a single time step, but on the manner in which successive errors tend to accumulate or cancel. How a specific form of differencing affects this latter aspect of accuracy is not subject to simple analysis. In the course of developing the difference equations of the previous section, a

number of variations in the form of such quantities as the boundary pressures and the mass flows was investigated. The final choice for these quantities was based on comparisons of calculated and analytic solutions for simple problems like the propagation and reflection of a plane shock (see Fig. 2). In this way, differencing procedures with large cumulative error were hopefully eliminated.

A more direct way in which accuracy is limited by the magnitudes of the space and time intervals is that transient phenomena occurring in times shorter than Δt or details of a flow pattern smaller than the size of a mesh cell will always be washed out.

The difference equations are subject to the Courant stability criterion⁴ $c\Delta t < \Delta x^*$ which requires that a disturbance moving at the local sound speed c may only affect adjacent mesh points in a single time cycle. A generally more restrictive condition for supersonic problems is that $u\Delta t < \Delta x$ and $v\Delta t < \Delta x$ since the difference equations do not provide a mechanism for the transfer of fluid between nonadjacent cells.

Explicit Eulerian difference equations are often unconditionally unstable with respect to small perturbations in the flow quantities, particularly at low velocity. Stability can be achieved by the addition of a fictitious viscous pressure⁵ to the hydrostatic pressure in the momentum and energy equations. Such viscous pressure terms cause a diffusion of momentum and energy which has a limiting effect on the gradients of these quantities and constitutes a source of entropy production through the conversion of kinetic to internal energy. Though the diffusion

*In the following we will set $\Delta x = \Delta y$.

caused by these terms contributes to the inaccuracy of a difference scheme, it serves the important function, in addition to its stabilizing effects, of smearing out discontinuities such as shock fronts, which enables the calculation of these phenomena without special treatment.⁵ Typically, discontinuities such as shock fronts are smeared over a three-cell width, so that a reduction in cell size will improve the sharpness of the discontinuity.

The dissipation terms of the difference equations described above are implicit rather than explicit and arise from the "repartitioning" of the energy and momentum in cells on the basis of total energy and momentum conservation after the mass flow, i.e. in Phase III of the calculation. The dissipative mechanisms involved can be illustrated by considering a box containing N distinct mass phases having different velocities and internal energies, and then allowing these to fuse into a single mass with one velocity and one internal energy. Originally the contents of the box could be described by the set of masses, velocities and specific internal energies,

$$m_k, \vec{v}_k, I_k, \quad k = 1, \dots, N$$

The initial momentum and internal energy are

$$\vec{P} = \sum_{k=1}^N m_k \vec{v}_k$$

$$IE_i = \sum_{k=1}^N m_k I_k$$

Since mass, energy, and momentum must be conserved, the final internal energy will be

$$IE_f = \sum_{k=1}^N m_k \left(\frac{1}{2} \vec{v}_k^2 + I_k \right) - \frac{\vec{P}^2}{2M}$$

where

$$M = \sum_{k=1}^N m_k$$

The change in internal energy will be

$$\begin{aligned} \Delta IE &= IE_f - IE_i = \frac{1}{2M} \sum_{j,k=1}^N \left(m_j m_k \vec{v}_k^2 - m_j m_k \vec{v}_j \cdot \vec{v}_k \right) \\ &= \frac{1}{2M} \sum_{j>k=1}^N m_j m_k \left(\vec{v}_k^2 + \vec{v}_j^2 - 2\vec{v}_j \cdot \vec{v}_k \right) \end{aligned}$$

Since $\vec{v}_k^2 + \vec{v}_j^2 - 2\vec{v}_j \cdot \vec{v}_k = (\vec{v}_k - \vec{v}_j)^2$ the change in internal energy, ΔIE , will be greater than or equal to zero and will, in fact, only vanish if all N initial velocities are equal. Therefore, the mixing of the component masses in general results in a conversion of kinetic to internal energy, a dissipative entropy producing process.

The form of the viscous pressure implicit in the difference equations may be obtained by converting these back to differential equations at the point (i,j) ,¹ retaining terms through first order in Δx

and Δy .^{*} That is, we let

$$\rho_{i,j} \rightarrow \rho, \quad E_{i,j} \rightarrow E, \quad u_{i,j} \rightarrow u, \quad v_{i,j} \rightarrow v$$

and replace flow quantities at neighboring points by appropriate Taylor expansions about (i,j) . In performing this reduction it is convenient to choose a definite flow direction, say in the positive u and v directions. The resultant differential equations are

$$\frac{\partial \rho}{\partial t} + \text{div}(\rho \vec{u}) = 0$$

$$\frac{\partial \rho u}{\partial t} + \text{div}(\rho u \vec{u}) + \frac{\partial p}{\partial x} = \frac{\partial}{\partial x} \left(\frac{1}{2} \rho u \Delta x \frac{\partial u}{\partial x} \right) + \frac{\partial}{\partial y} \left(\frac{1}{2} \rho v \Delta y \frac{\partial u}{\partial y} \right)$$

$$\frac{\partial \rho v}{\partial t} + \text{div}(\rho v \vec{u}) + \frac{\partial p}{\partial y} = \frac{\partial}{\partial y} \left(\frac{1}{2} \rho v \Delta y \frac{\partial v}{\partial y} \right) + \frac{\partial}{\partial x} \left(\frac{1}{2} \rho u \Delta x \frac{\partial v}{\partial x} \right)$$

$$\frac{\partial \rho E}{\partial t} + \text{div}(\rho E \vec{u}) + \text{div}(p \vec{u}) = \frac{\partial}{\partial x} \left(\frac{1}{2} \rho u \Delta x \frac{\partial E}{\partial x} \right) + \frac{\partial}{\partial y} \left(\frac{1}{2} \rho v \Delta y \frac{\partial E}{\partial y} \right)$$

Apart from the first order terms on the right, these are the Eulerian hydrodynamic equations. That they can be obtained from the difference equations justifies the three phase difference scheme.

The viscous pressure is seen from the momentum equations to have the appearance of a tensorial pressure resulting from viscous interactions,

^{*}The first order terms in Δt do not seem to have as important a role as the viscosity terms, undoubtedly because $\Delta t \ll \Delta x$. They are also primarily diffusion-like quantities.

$$\frac{1}{2} \rho \begin{bmatrix} u \Delta x \frac{\partial u}{\partial x} & v \Delta y \frac{\partial u}{\partial y} \\ u \Delta x \frac{\partial v}{\partial x} & v \Delta y \frac{\partial v}{\partial y} \end{bmatrix}$$

However, written in the diadic form $\frac{1}{2} \rho \vec{u} \Delta \vec{r} \cdot \nabla \vec{u}$, where $\Delta \vec{r} = \Delta x \vec{i} + \Delta y \vec{j}$, it is seen that this pressure is not an invariant form due to the presence of the fixed vector, $\Delta \vec{r}$. Its elements are large only when the velocity and its gradients are large. (The diffusion terms in the energy equation above are also small when v is small.) Thus in regions of near stagnation the viscosity will be ineffective and the instabilities of the difference equations will cause an exponential growth of any perturbations to the solution. However, once the velocity has reached a magnitude comparable to the local sound speed, the viscosity will act to limit further growth of the instability. This type of bounded instability is illustrated by Fig. 2a where the calculated velocity for a one dimensional steady shock reflected from a barrier is shown. The shock front is moving to the left and the velocity behind it should be zero. However, instabilities cause large oscillations in this quantity.

The difficulties with the difference equations at low velocities can be alleviated by supplementing the implicit viscous pressure with an explicit term in the momentum and energy equations. A satisfactory way of accomplishing this is to add such a term to the pressure at a cell boundary if the fluid speed is found to be small compared to the sound speed

at this boundary. For example, assuming the fluid is a perfect gas and considering the right-hand boundary of cell (i,j) , one could make a test to see if

$$2c_{i+\frac{1}{2},j}^2 = \gamma(\gamma - 1) (I_{i,j} + I_{i+1,j}) < A[(u_{i,j} + u_{i+1,j})^2 + (v_{i,j} + v_{i+1,j})^2] \quad (13)$$

where $c_{i+\frac{1}{2},j}$ is the sound speed at the boundary and A is a constant greater than one. If the inequality is satisfied no additional viscous term is necessary. If it is not, a Landshoff type viscous pressure⁶ could be added to the boundary pressure, i.e.,

$$(p_{i,j} + p_{i+1,j}) \rightarrow (p_{i,j} + p_{i+1,j}) - B c_{i+\frac{1}{2},j} \Delta x (p_{i,j} + p_{i+1,j}) (v_{i+1,j} - v_{i,j}) \quad (14)$$

With such a prescription the difference equations will remain stable at fluid speeds of a few percent of the local speeds of sound. Optimum constants A and B can be determined from tests with simple one dimensional problems. For the calculations in Section IV of this report where the fluid was air and $\gamma = 1.4$, A and B were 1.5 and 0.3, respectively.

Figures 2b and 2a compare the calculated velocity of a steady shock which has been reflected from a rigid wall, with and without a supplementary viscous pressure. The improved stability is self evident.

As a final remark, it might be noted that negative internal energies can arise under special circumstances in the course of a calculation as in the PIC method. This is particularly true during the initial time

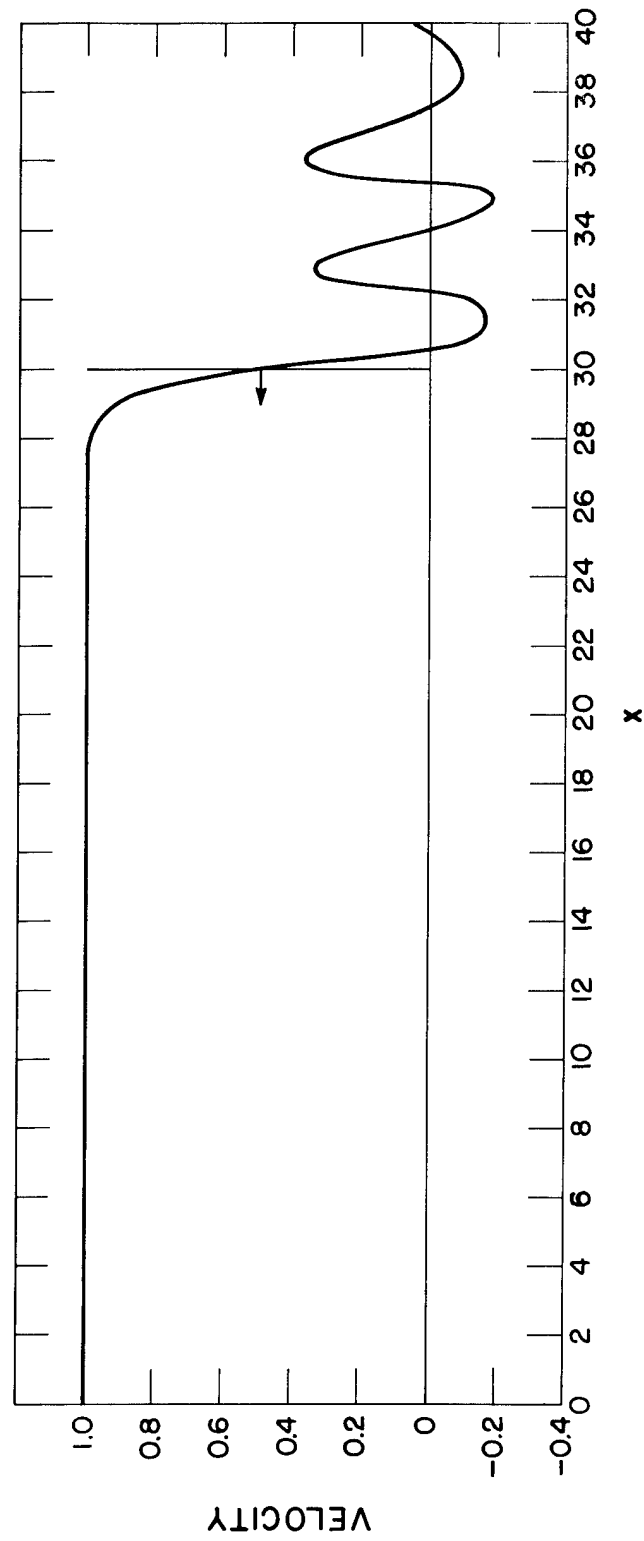


Figure 2a. Plot of a calculated velocity profile vs position for a plane shock reflected from a rigid wall using no explicit viscous pressure. The true shock position is indicated by a vertical line with an arrow specifying direction of motion.

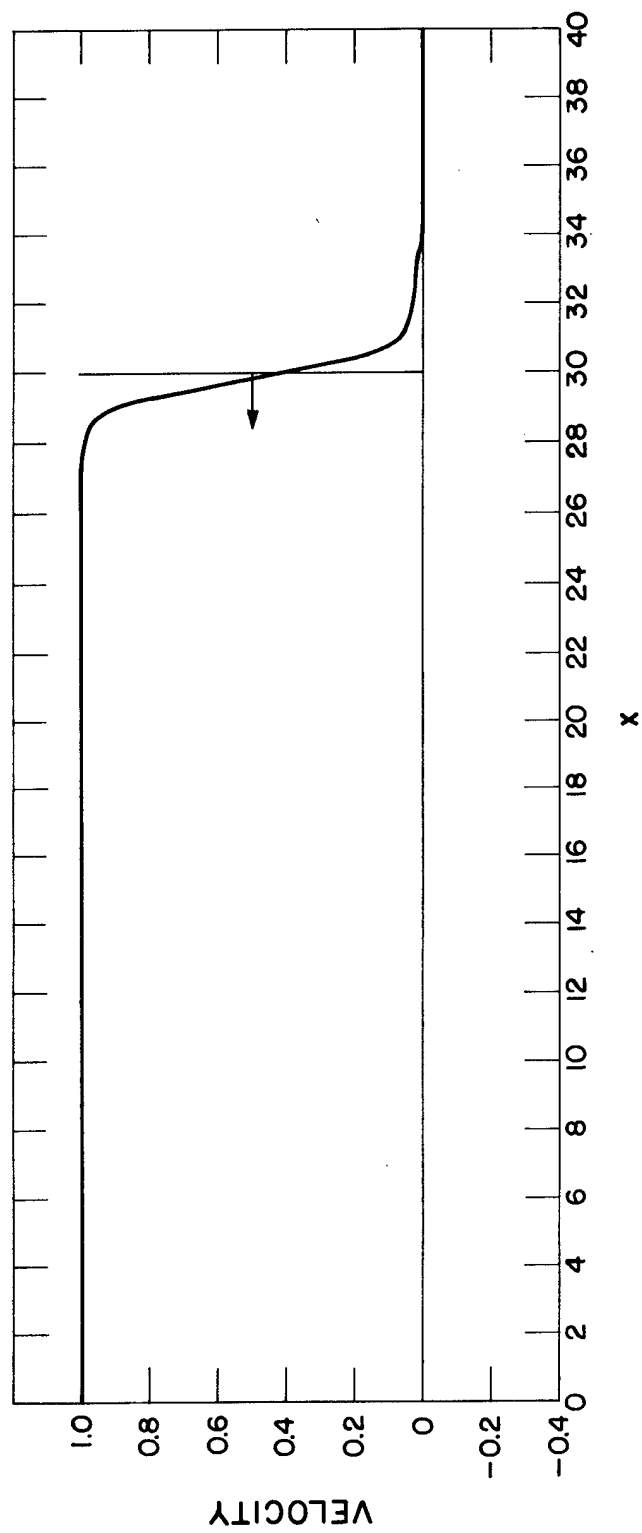


Figure 2b. Same calculation as in Fig. 2a, but with an explicit viscous pressure corresponding to $A = 2.5$ and $B = 0.5$.

cycles when a cold fluid at rest is acted upon by some driving force. In this case, the source of the negative internal energy can be found in Eqs. (5), (6), and (7) of the Phase I calculation. If initially $u_{i,j}^{(n)}$, $v_{i,j}^{(n)}$, and $E_{i,j}^{(n)}$ are zero but a pressure gradient exists, $\tilde{u}_{i,j}^{(n)}$ and $\tilde{v}_{i,j}^{(n)}$ will not vanish but $\tilde{E}_{i,j}^{(n)}$ will in general remain zero since the time n velocities are used to calculate the energy fluxes. Therefore one will obtain

$$\tilde{I}_{i,j}^{(n)} = \tilde{E}_{i,j}^{(n)} - \frac{1}{2} \left[\tilde{u}_{i,j}^{(n)2} + \tilde{v}_{i,j}^{(n)2} \right] \leq 0$$

since $\tilde{E}_{i,j}^{(n)} = 0$. This result is due to a somewhat improper phasing between the momentum Eqs. (5) and (6) and the energy Eq. (7) and could be largely corrected by replacing the velocities in the latter by the just calculated tilde velocities. However these negative internal energies do not seem to persist for more than a few time cycles and have not led to any difficulties, so their occasional occurrence has been ignored.

III. BOUNDARY CONDITIONS AND THE TREATMENT OF SEVERAL FLUIDS

For a single fluid the most common types of boundary conditions fall into two categories, those at open ends of the mesh across which fluid can enter or leave and those at rigid barriers within or at the extremities of the mesh. The different cases which fall under each category will be enumerated below.

A. Boundary Conditions at Open Ends of a Mesh

1. Prescribed Input

Suppose fluid is flowing into a rectangular mesh from the left-hand side. Then the left side $(\frac{1}{2}, j)$ of cell $(1, j)$ forms the boundary with the exterior region. It is seen from Eqs. (5), (7), (8), (9), and (10) that the following quantities must be known in order to apply the difference equations:

$$P_{\frac{1}{2}, j}, v_{\frac{1}{2}, j}, \Delta M_{\frac{1}{2}, j}, \tilde{u}_{0, j}, \tilde{v}_{0, j}, \tilde{E}_{0, j}, \tilde{v}_{-1, j}, \rho_{-1, j}$$

That is, we must know the energy and momentum flux into the cell from the outside and the mass transport quantities. The indices $(0, j)$ and $(-1, j)$ refer to fictitious cells to the left of mesh cell $(1, j)$. The input boundary conditions are prescribed by specifying the above eight quantities for each time cycle. More simply, it is usually possible to prescribe the nature of the flow to the left of cell $(1, j)$. If $\rho_{-1, j}$, $v_{-1, j}$, $\rho_{0, j}$, $u_{0, j}$, $v_{0, j}$, $E_{0, j}$ are given for the fictitious external cells $(-1, j)$ and $(0, j)$ each cycle, the boundary quantities at $(\frac{1}{2}, j)$ can be calculated with the equations of Section II.

2. Continuous Outflow

In order to allow fluid to flow out of a mesh, the external boundary must be sufficiently far from any source of disturbance so that the flow pattern can be extrapolated to the outside. The simplest example of this situation is where the flow is uniform, say at the right-hand end of the mesh. If the mesh is N cells long, the conditions in a fictitious cell

$(N + 1, j)$ to the right of the last cell (N, j) should always be the same as in (N, j) . Suitable boundary conditions can be achieved by allowing for cell $(N + 1, j)$ and setting

$$\tilde{u}_{N+1,j} = \tilde{u}_{N,j}, \quad \tilde{v}_{N+1,j} = \tilde{v}_{N,j}, \quad \tilde{E}_{N+1,j} = \tilde{E}_{N,j}$$

at the end of Phase I of each cycle of calculation, and setting

$$\rho_{N+1,j}^{(n+1)} = \rho_{N,j}^{(n+1)}, \quad u_{N+1,j}^{(n+1)} = u_{N,j}^{(n+1)}, \quad v_{N+1,j}^{(n+1)} = v_{N,j}^{(n+1)}, \quad E_{N+1,j}^{(n+1)} = E_{N,j}^{(n+1)}$$

at the end of Phase III.

B. Interactions with Rigid Barriers

1. Barriers at Cell Boundaries

Barriers at cell boundaries occur most commonly when the mesh consists of a channel to which the fluid is confined or in cylindrical coordinates where the axis of symmetry can be represented by a rigid barrier. The boundary conditions are determined by the necessity that there must be no energy flux or fluid flow across the barrier. This will be assured if the velocity normal to the barrier is zero. The momentum flux at the obstacle boundary is not zero and can be obtained approximately by extrapolating the pressure to the wall. If the mesh is fine, the pressure at the barrier can be chosen as that at the center of the cell bounded by the obstacle.

By way of an example, assume the right-hand side of cell (i, j) represents the boundary with a rigid obstacle. As in the case of the

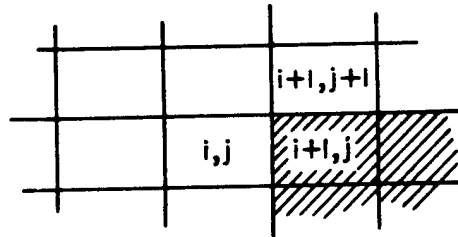
open-ended boundary, a fictitious mesh cell $(i + 1, j)$ can be assumed and its state prescribed in terms of that of cell (i, j) so that application of the equation of Section II will automatically produce the correct boundary conditions. The prescription for cell $(i + 1, j)$ is that the density and specific energy must at all times be the same as in cell (i, j) , but the velocity must be the mirror image of that in (i, j) . Thus at the end of Phase I one can set

$$\tilde{E}_{i+1,j} = \tilde{E}_{i,j}, \quad \tilde{u}_{i+1,j} = -\tilde{u}_{i,j}, \quad \tilde{v}_{i+1,j} = \tilde{v}_{i,j}$$

and at the end of Phase III,

$$\rho_{i+1,j}^{(n+1)} = \rho_{i,j}^{(n+1)}, \quad E_{i+1,j}^{(n+1)} = E_{i,j}^{(n+1)}, \quad u_{i+1,j}^{(n+1)} = -u_{i,j}^{(n+1)}, \quad v_{i+1,j}^{(n+1)} = v_{i,j}^{(n+1)}$$

In the case that the obstacle has a corner as shown by the shaded area below,



the fictitious cell $(i + 1, j)$ will be assigned two different sets of variables depending on whether computations are being done in cell (i, j) or $(i + 1, j + 1)$.

The use of a fictitious cell with assigned variables is not actually necessary though it often is convenient. In practice one can test to see if calculations are being made in a "boundary cell" like (i, j) shown above, and if so, merely set $p_{i+\frac{1}{2},j} = p_{i,j}$ and $\tilde{u}_{i+\frac{1}{2},j}^{(n)} = \tilde{u}_{i+\frac{1}{2},j}^{(n+1)} = 0$.

If this second procedure is followed, it has been found that setting $\tilde{u}_{i+1,j} = + \tilde{u}_{i,j}$ for use in the mass flow calculation improves the accuracy of the computations.

2. Arbitrary Linear Barriers Within a Cell

As in the previous case of a barrier at a cell boundary, the difference equations applicable when the barrier is within a cell are determined by the requirements that no energy flux or mass may cross the boundary. In fact, treatment of a barrier at a cell boundary is merely a special case of what will be discussed here.

Placing a barrier within a mesh cell^{*} has two primary effects. It shifts the center of mass from the cell center to some point nearer the cell boundary, and it reduces the effective length of the cell in at least one direction. In general, the hydrodynamic parameters describing the state of the fluid within a mesh cell refer specifically to the center of mass of the cell. When making an interpolation of some quantity between cells, one in fact should interpolate between centers of mass. For non-fractional cells the center of mass will either coincide with the cell center, as in Cartesian coordinates, or be sufficiently close to the cell center so that the difference can be neglected. An example of the latter situation is cylindrical coordinates where even for cells adjacent to the axis of symmetry the center of mass differs from the cell center by only two tenths of the radial cell dimension. Since

^{*}Cells containing or adjacent to a barrier will be called "fractional cells."

the center of mass of fractional cells are in general well displaced from the cell center, we should by rights calculate those quantities needed at cell boundaries by interpolation with respect to centers of mass. However the errors involved in interpolating with respect to cell centers are felt to be minor, even for fractional cells; and so in practice, these effects of center-of-mass displacement have been neglected.

The reduction of the effective cell dimensions in fractional cells is a more serious matter, particularly if the center-of-mass displacements are disregarded. This is because the stability requirements for the difference equations at such a cell may now be violated with the resultant appearance of large localized fluctuations. Therefore special procedures must be adopted to minimize these difficulties.

There are twelve distinct types of fractional cells containing single linear barriers which must be treated individually. They are of the following form (Fig. 3), where the shaded area represents the presence of a rigid obstacle:

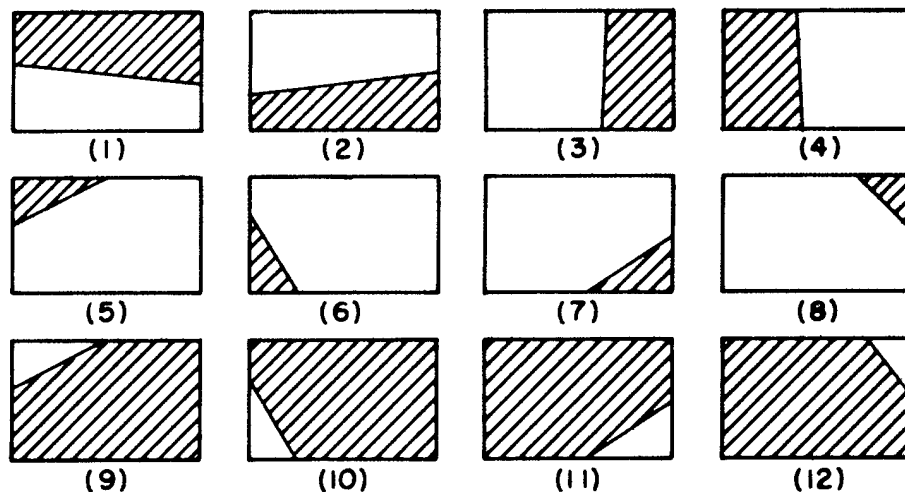


Figure 3. Types of fractional cells.

For each fractional cell a set of five geometrical quantities $f_{i,j}$, $A_{i-\frac{1}{2},j}$, $A_{i,j-\frac{1}{2}}$, $A_{i+\frac{1}{2},j}$, and $A_{i,j+\frac{1}{2}}$ will be needed. $f_{i,j}$ is the fraction of the total cell "volume," $\Delta x \Delta y$, which is occupied by fluid; $A_{i-\frac{1}{2},j}$ is the fraction of the "area" of cell side $(i - \frac{1}{2}, j)$ which is open to flow; etc.

Using the above quantities, difference equations for fractional cells can be obtained from those for "full" cells given in Section II B by multiplying mass and energy transport terms at a given cell side by the corresponding fractional area, A , and by multiplying the densities occurring explicitly in Eqs. (5, 6, 7, 8, 10, 11, 12) by $f_{i,j}$. The pressures in Eqs. (5) and (6) now represent averages of pressures at the perimeter of the region occupied by fluid in the fractional cell. To avoid overly complicating the computing procedure, pressures have been calculated as if the fractional cell were effectively rectangular, with the pressure at cell boundaries taken, as before, to be the simple average of the pressures in the cells on either side, and the pressure at the obstacle face being taken as that within the fractional cell. The pressure difference in Eq. (5) must be multiplied by the larger of the fractional areas $A_{i-\frac{1}{2},j}$ and $A_{i+\frac{1}{2},j}$, and that of Eq. (6) by the larger of $A_{i,j-\frac{1}{2}}$ and $A_{i,j+\frac{1}{2}}$.

With these changes, Eqs. (5) through (9) become

$$\tilde{u}_{i,j}^{(n)} = \tilde{u}_{i,j}^{(n)} - \frac{p_{i+\frac{1}{2},j}^{(n)} - p_{i-\frac{1}{2},j}^{(n)}}{\Delta x} \frac{\Delta t}{\rho_{i,j}^{(n)}} \frac{\text{Max}(A_{i+\frac{1}{2},j}, A_{i-\frac{1}{2},j})}{f_{i,j}} \quad (5')$$

$$\tilde{v}_{i,j}^{(n)} = \tilde{v}_{i,j}^{(n)} - \frac{p_{i,j+\frac{1}{2}}^{(n)} - p_{i,j-\frac{1}{2}}^{(n)}}{\Delta y} \frac{\Delta t}{\rho_{i,j}^{(n)}} \frac{\text{Max}(A_{i,j+\frac{1}{2}}, A_{i,j-\frac{1}{2}})}{f_{i,j}} \quad (6')$$

$$\begin{aligned} \tilde{E}_{i,j}^{(n)} = E_{i,j}^{(n)} - & \left[\frac{A_{i+\frac{1}{2},j} p_{i+\frac{1}{2},j}^{(n)} u_{i+\frac{1}{2},j}^{(n)} - A_{i-\frac{1}{2},j} p_{i-\frac{1}{2},j}^{(n)} u_{i-\frac{1}{2},j}^{(n)}}{\Delta x} \right. \\ & \left. + \frac{A_{i,j+\frac{1}{2}} p_{i,j+\frac{1}{2}}^{(n)} v_{i,j+\frac{1}{2}}^{(n)} - A_{i,j-\frac{1}{2}} p_{i,j-\frac{1}{2}}^{(n)} v_{i,j-\frac{1}{2}}^{(n)}}{\Delta y} \right] \frac{\Delta t}{f_{i,j} \rho_{i,j}^{(n)}} \end{aligned} \quad (7')$$

$$f_{i,j} \rho_{i,j}^{(n+1)} \Delta x \Delta y = f_{i,j} \rho_{i,j}^{(n)} \Delta x \Delta y - \Delta M_{i+\frac{1}{2},j}^{(n)} + \Delta M_{i-\frac{1}{2},j}^{(n)} - \Delta M_{i,j+\frac{1}{2}}^{(n)} + \Delta M_{i,j-\frac{1}{2}}^{(n)} \quad (8')$$

$$\Delta M_{i+\frac{1}{2},j}^{(n)} = A_{i+\frac{1}{2},j} \rho_{i+\frac{1}{2},j}^{(n)} \tilde{u}_{i+\frac{1}{2},j} \Delta y \Delta t \quad (9')$$

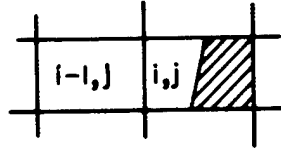
$$\Delta M_{i,j+\frac{1}{2}}^{(n)} = A_{i,j+\frac{1}{2}} \rho_{i,j+\frac{1}{2}}^{(n)} \tilde{v}_{i,j+\frac{1}{2}} \Delta x \Delta t$$

In Eqs. (10), (11), and (12) we merely replace each $\rho_{i,j}$ by $f_{i,j} \rho_{i,j}$. All other equations, for instance those defining the $\rho_{i+\frac{1}{2},j}^{(n)}$ and $u_{i+\frac{1}{2},j}^{(n)}$ appearing in Eq. (9) are treated in the same manner as in the case of full cells with a barrier along a cell boundary, as described in III B1 above.

Another procedure which can be used without undue error in the calculation of tilde quantities in fractional cells is to regard the cell as full-fractional as in III B1 for the purpose of obtaining $\tilde{u}_{i,j}$ and $\tilde{v}_{i,j}$. This produces a somewhat different transfer of momentum to the obstacle than results from the use of Eqs. (5') and (6'), but does not seriously affect the flow pattern if the mesh is not too coarse. This alternate differencing cannot be applied to the calculation of $\tilde{E}_{i,j}$ in fractional

cells since it would result in a violation of energy conservation. No energy can be transferred to the obstacle.

In some instances the fractional volumes of cells of type (1), (2), (3), or (4) may be sufficiently small so that stability requirements are violated. The second treatment of the tilde velocities is then particularly useful. In addition, that for the tilde energy must be changed from Eq. (7') to prevent instabilities. One such modification, which is not in contradiction with energy conservation, is to allow only the fraction $f_{i,j}$ of the energy crossing the fully open boundary of these types of cells to enter or leave the fractional cell, the remaining fraction $(1 - f_{i,j})$ being returned to the cell from which the energy flowed. For example, for a type (3) cell shown below the \tilde{E} equations would become:



$$\begin{aligned} \tilde{E}_{i,j}^{(n)} &= E_{i,j}^{(n)} - \left[\frac{0 - p_{i-\frac{1}{2},j}^{(n)} u_{i-\frac{1}{2},j}^{(n)} f_{i,j}}{\Delta x} \right. \\ &\quad \left. + \frac{A_{i,j+\frac{1}{2}} p_{i,j+\frac{1}{2}}^{(n)} v_{i,j+\frac{1}{2}}^{(n)} - A_{i,j-\frac{1}{2}} p_{i,j-\frac{1}{2}}^{(n)} v_{i,j-\frac{1}{2}}^{(n)}}{\Delta y} \right] \frac{\Delta t}{\rho_{i,j}^{(n)} f_{i,j}} \\ \tilde{E}_{i-1,j}^{(n)} &= E_{i-1,j}^{(n)} - \left[\frac{p_{i-\frac{1}{2},j}^{(n)} u_{i-\frac{1}{2},j}^{(n)} f_{i,j} - p_{i-\frac{3}{2},j}^{(n)} u_{i-\frac{3}{2},j}^{(n)}}{\Delta x} \right. \\ &\quad \left. + \frac{p_{i-1,j+\frac{1}{2}}^{(n)} v_{i-1,j+\frac{1}{2}}^{(n)} - p_{i-1,j-\frac{1}{2}}^{(n)} v_{i-1,j-\frac{1}{2}}^{(n)}}{\Delta y} \right] \frac{\Delta t}{\rho_{i-1,j}^{(n)}} \end{aligned}$$

The calculation of a viscous pressure at the boundaries of fractional cells can be accomplished similarly to that for a normal cell with the

following additional prescription:

- a. If the cell side has part of its area open for fluid flow into an adjacent cell, calculate the viscous pressure terms as if this side were entirely unobstructed.
- b. If a side of cell (i,j) is entirely closed to fluid flow, Eqs. (13) and (14) should be replaced by

$$\frac{1}{2} \sigma_{i,j}^2 < A \left[u_{i,j}^2 + v_{i,j}^2 \right] \quad (13')$$

and

$$(p_{i,j} + p_{i+1,j}) \rightarrow 2p_{i,j} - 4B c_{i,j} \rho_{i,j} v_{i,j} \quad (14')$$

The treatment of fractional cells described above is rather crude and can be improved upon in many ways. However it has the virtue of relative simplicity and does not deter from accuracy as long as the Eulerian mesh is made fine compared to the obstacle.

C. Two Material Cells

The presence of several distinct fluids separated by interfaces within the confines of an Eulerian mesh increases the difficulty of such calculations many fold. Special treatment, similar to that for "fractional" cells in one fluid problems, must be given to cells containing more than one fluid at each phase of the calculation; and, in addition, a method for moving the interface must be prescribed. In the following, a method for performing Eulerian calculations in cells containing two fluids will be outlined. This procedure has been tested with reasonable success in several trial problems. It is characterized by an indirect method for moving the

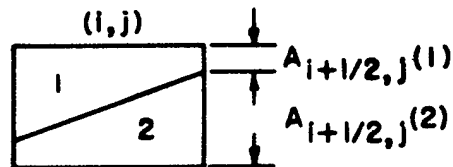
fluid interface. This is as opposed to a direct movement of a boundary by means of the explicit motion of points which specify its position.

A single fluid in an Eulerian mesh cell is characterized by a density, velocity, and internal energy "located" at the cell center. When two fluids are present in such a cell, each will have a distinct density, internal energy, and parameter specifying the fraction of the cell each occupies. A distinct velocity may also be given to each material, with the restriction that the components normal to the interface be equal, in order to allow for slippage at the interface. This situation will not be considered here, and a single velocity for both fluids in a given cell will be assumed. In addition the assumption of continuity of pressure will be made so that there is a single pressure in the cell possessed by both fluids. The velocity and pressure of a multi-fluid cell is thus treated as in a single fluid cell and is assumed "located" at the cell center. Although this point will in general no longer be the cell center of mass, errors due to this deviation should not be important. Finally, the interface segment within a single cell will always be assumed to be a straight line. A specification of which pair of cell boundaries this line intersects and the position of the intersection points are required to complete the information about the two fluid cell.

The complexity of the equations of motion for a two fluid cell depend on the degree of precision one wants to incorporate in them. Ideally each material in a two fluid cell should be treated independently as a single fluid in a "fractional cell" except for such constraints as continuity of

pressure. This will in fact be done in Phases II and III of the calculation, but the cell will be treated here as a single full cell in Phase I.

Consider an arbitrary two fluid cell such as that shown below:



As with a single fluid cell, it is assumed that at time $n\Delta t$ the density, mass, and specific energy of both fluids are known and that a single pressure and velocity has also been assigned to each cell. The Phase I equations, in which no mass flow occurs, can be deduced from Eqs. (2) and (3) to be

$$\tilde{u}_{i,j}^{(n)} = u_{i,j}^{(n)} - \frac{p_{i+\frac{1}{2},j}^{(n)} - p_{i-\frac{1}{2},j}^{(n)}}{\Delta x} \frac{\Delta t}{\rho_1^{(n)} f_1^{(n)} + \rho_2^{(n)} f_2^{(n)}} \quad (15)$$

$$\tilde{v}_{i,j}^{(n)} = v_{i,j}^{(n)} - \frac{p_{i,j+\frac{1}{2}}^{(n)} - p_{i,j-\frac{1}{2}}^{(n)}}{\Delta y} \frac{\Delta t}{\rho_1^{(n)} f_1^{(n)} + \rho_2^{(n)} f_2^{(n)}} \quad (16)$$

$$\begin{aligned} & \rho_{i,j}^{(n)(1)} f_{i,j}^{(n)(1)} \left[\tilde{E}_{i,j}^{(n)(1)} - E_{i,j}^{(n)(1)} \right] + \rho_{i,j}^{(n)(2)} f_{i,j}^{(n)(2)} \left[\tilde{E}_{i,j}^{(n)(2)} - E_{i,j}^{(n)(2)} \right] \\ &= - \Delta t \left[\frac{p_{i+\frac{1}{2},j}^{(n)} u_{i+\frac{1}{2},j}^{(n)} - p_{i-\frac{1}{2},j}^{(n)} u_{i-\frac{1}{2},j}^{(n)}}{\Delta x} + \frac{p_{i,j+\frac{1}{2}}^{(n)} v_{i,j+\frac{1}{2}}^{(n)} - p_{i,j-\frac{1}{2}}^{(n)} v_{i,j-\frac{1}{2}}^{(n)}}{\Delta y} \right] \end{aligned} \quad (17)$$

where $f_{i,j}^{(n)(1)}$ and $f_{i,j}^{(n)(2)}$ are the fractional volumes of cell (i,j) at

"time" n occupied by fluids (1) and (2), respectively. If $R_{i,j}^{(n)(1)}$ and $R_{i,j}^{(n)(2)}$ are the respective masses of the two fluids in cell (i,j) divided

by the volume $\Delta x \Delta y$, then

$$f_{i,j}^{(n)}(1) = \frac{R_{i,j}^{(n)}(1)}{\rho_{i,j}^{(n)}(1)}$$

$$f_{i,j}^{(n)}(2) = \frac{R_{i,j}^{(n)}(2)}{\rho_{i,j}^{(n)}(2)}$$

The $R_{i,j}$'s and $\rho_{i,j}$'s are not all independent since

$$f_{i,j}^{(n)}(1) + f_{i,j}^{(n)}(2) = 1$$

Equation (17) does not permit an independent determination of $\tilde{E}_{i,j}^{(n)}(1)$ and $\tilde{E}_{i,j}^{(n)}(2)$. Unless these are calculated in a manner similar to that for fractional one fluid cells discussed above, an additional assumption must be made at this point. One such is that the energy brought into the cell by the flux terms in Eq. (17) is distributed uniformly across the cell. Then each fluid is incremented in energy by an amount proportional to its fractional volume so that

$$\begin{aligned} \tilde{E}_{i,j}^{(n)}(\alpha) = E_{i,j}^{(n)}(\alpha) - \frac{\Delta t}{\rho_{i,j}^{(n)}(\alpha)} & \left[\frac{p_{i+\frac{1}{2},j}^{(n)} u_{i+\frac{1}{2},j}^{(n)} - p_{i-\frac{1}{2},j}^{(n)} u_{i-\frac{1}{2},j}^{(n)}}{\Delta x} \right. \\ & \left. + \frac{p_{i,j+\frac{1}{2}}^{(n)} v_{i,j+\frac{1}{2}}^{(n)} - p_{i,j-\frac{1}{2}}^{(n)} v_{i,j-\frac{1}{2}}^{(n)}}{\Delta y} \right], \quad \alpha = 1, 2 \end{aligned} \quad (18)$$

The assumption leading to the above equation is, of course, arbitrary.

The calculation of the mass flows in Phase II is similar to that for the single fluid fractional cell described above. There are now two separate sets of mass flows, however, one for each fluid. In order to avoid

extrapolation of densities beyond fluid interfaces, mass flows in multi-fluid problems have used boundary densities which are simply the density of the cell from which the fluid flows. Taking into account the area available for each fluid flow across a given cell boundary as determined by the position of the interface in the cell, we have for instance for side $(i+\frac{1}{2}, j)$ of the two fluid cell pictured above:

If

$$\tilde{u}_{i,j}^{(n)} + \tilde{u}_{i+1,j}^{(n)} > 0$$

and

$$\tilde{u}_{i+\frac{1}{2},j}^{(n)} = \tilde{u}_{i,j}^{(n)} + \frac{\tilde{u}_{i+1,j}^{(n)} - \tilde{u}_{i-1,j}^{(n)}}{4} > 0$$

then

$$\Delta M_{i+\frac{1}{2},j}^{(n)}(\alpha) = \tilde{u}_{i+\frac{1}{2},j}^{(n)} \rho_{i,j}^{(n)}(\alpha) A_{i+\frac{1}{2},j}^{(n)}(\alpha) \Delta Y \Delta t, \quad \alpha = 1,2$$

if

$$\tilde{u}_{i,j}^{(n)} + \tilde{u}_{i+1,j}^{(n)} < 0$$

and

$$\tilde{u}_{i+\frac{1}{2},j}^{(n)} = \tilde{u}_{i+1,j}^{(n)} - \frac{\tilde{u}_{i+2,j}^{(n)} - \tilde{u}_{i,j}^{(n)}}{4} < 0$$

then

$$\Delta M_{i+\frac{1}{2},j}^{(n)}(\alpha) = \tilde{u}_{i+\frac{1}{2},j}^{(n)} \rho_{i+1,j}^{(n)}(\alpha) A_{i+\frac{1}{2},j}^{(n)}(\alpha) \Delta Y \Delta t, \quad \alpha = 1,2$$

and otherwise

$$\Delta M_{i+\frac{1}{2},j}^{(n)}(\alpha) = 0, \quad \alpha = 1,2$$

In these equations, $A_{i+\frac{1}{2},j}^{(n)}(\alpha)$ is the fractional area of side $(i+\frac{1}{2},j)$ of cell (i,j) available for the flow of fluid α . For two fluids

$$A_{i+\frac{1}{2},j}^{(n)}(1) + A_{i+\frac{1}{2},j}^{(n)}(2) = 1$$

If a fluid has no contact with a cell boundary, its fractional area at that boundary will be zero.

These considerations of the mass flow across side $(i+\frac{1}{2},j)$ of the cell illustrated above can easily be extended to the other three sides and to other two fluid configurations. The procedure can be seen to have one serious limitation. If there were flow upward across the top, $(i,j+\frac{1}{2})$, of cell (i,j) , all of mass (1) would have to vacate this cell before any of mass (2) could enter cell $(i,j+1)$. Thus the method of calculation introduces local irregularities into the interface surface, though on the average the boundary will follow its proper course. This difficulty can be remedied by calculating the mass flows on the basis of the volume of one cell which is transported to another. The mass flow would then just be equal to the masses originally contained in this small volume.

The final step in the mass flow calculation for a two fluid cell is to check that the existing masses do not exceed the total mass originally in the cell. If it should for one of the fluids, each outgoing mass flow for that material must be reduced proportionally to its originally calculated value so that the sum of the outgoing flows exactly equals the total mass originally present. For example, if the total mass of material (1) is $M_{i,j}^{(1)}$ and the outgoing mass flows are

$$\Delta M_{i,j-\frac{1}{2}}^{(1)} < 0$$

$$\Delta M_{i+\frac{1}{2},j}^{(1)} > 0$$

$$M_{i,j}^{(1)} < \Delta M_{i+\frac{1}{2},j}^{(1)} - \Delta M_{i,j-\frac{1}{2}}^{(1)}$$

then the replacement must be made

$$\Delta M_{i,j-\frac{1}{2}}^{(1)} \rightarrow r \Delta M_{i,j-\frac{1}{2}}^{(1)}$$

$$\Delta M_{i+\frac{1}{2},j}^{(1)} \rightarrow r \Delta M_{i+\frac{1}{2},j}^{(1)}$$

where

$$r \equiv \frac{M_{i,j}^{(1)}}{\Delta M_{i+\frac{1}{2},j}^{(1)} - \Delta M_{i,j-\frac{1}{2}}^{(1)}}$$

The third phase of the two fluid calculation is essentially the same as in the single material case. Equations (8), (10), (11), and (12) are still relevant except that it is the "mass" (per volume $\Delta x \Delta y$)

$$R_{i,j}^{(n)} \equiv f_{i,j}^{(n)} \rho_{i,j}^{(n)} \quad (19)$$

which must replace the densities $\rho_{i,j}$ which explicitly appear in these equations. It should be noted that for cells containing only a single material $R_{i,j}^{(n+1)} = \rho_{i,j}^{(n+1)}$, while for multi-material cells the new densities $\rho_{i,j}^{(n+1)}(\alpha)$ are still unknown at this point of the calculation. The third phase of the calculation must further contain a test, after the calculation of the new $R_{i,j}$ quantities, to see whether a given cell has remained a one of two fluid cell, or whether a single material cell has become a two

material cell, or vice versa. If no change in cell structure has occurred, no further work is necessary. But if a one material cell has become a two material cell, provision must be made to determine the "type" of cell in accordance with Fig. 3, locate the interface, and calculate the densities; while if the reverse is true, these special considerations are no longer necessary.

As was stated above, at the end of the Phase III calculation the densities in multifluid cells are still unknown and must be obtained. In addition the new position of the boundary between materials must be found and a method given for computing the pressure in these cells. These quantities could be calculated directly on the basis of a procedure which involves the explicit movement of fluid interface with interpolated velocities during the Phase II calculations. However the necessity of keeping the interface motion compatible with the mass flows causes this to be a complicated, though not intrinsically difficult process. As an alternative, one can first obtain the pressure and densities in the cell as a consequence of the assumption of continuity of pressure and then use this information to locate the intercepts of the interfluid boundary with the cell sides. By way of example, if the two fluids were perfect gases obeying the equations of state,

$$p(1) = (\gamma_1 - 1) \rho(1) I(1)$$

and

$$p(2) = (\gamma_2 - 1) \rho(2) I(2)$$

where I is the specific internal energy, the continuity of pressure in the

two material cell (i,j) requires

$$(\gamma_1 - 1) \rho_{i,j}^{(1)} I_{i,j}^{(1)} = (\gamma_2 - 1) \rho_{i,j}^{(2)} I_{i,j}^{(2)}$$

Here all quantities but the $\rho_{i,j}^{(\alpha)}$ are known at the end of the Phase III calculation. Using the relations

$$\rho_{i,j}^{(\alpha)} = \frac{R_{i,j}^{(\alpha)}}{f_{i,j}^{(\alpha)}}, \quad \alpha = 1, 2$$

and

$$f_{i,j}^{(1)} + f_{i,j}^{(2)} = 1$$

one can obtain an equation for $f_{i,j}^{(1)}$

$$(\gamma_1 - 1) \frac{R_{i,j}^{(1)}}{f_{i,j}^{(1)}} I_{i,j}^{(1)} = (\gamma_2 - 1) \frac{R_{i,j}^{(2)}}{1 - f_{i,j}^{(1)}} I_{i,j}^{(2)}$$

whose solution is

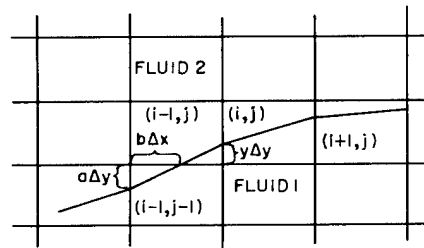
$$f_{i,j}^{(1)} = \frac{(\gamma_1 - 1) R_{i,j}^{(1)} I_{i,j}^{(1)}}{(\gamma_1 - 1) R_{i,j}^{(1)} I_{i,j}^{(1)} + (\gamma_2 - 1) R_{i,j}^{(2)} I_{i,j}^{(2)}}$$

Once $f_{i,j}^{(1)}$ is known, $\rho_{i,j}^{(1)}$, $\rho_{i,j}^{(2)}$, and $\rho_{i,j}$ can be found immediately.

In practice, if the equations of state for the materials are complicated and the cell size small compared to the distance over which significant changes in parameters occur, it may be adequate and easier to extrapolate the densities in multifluid cells from those in single fluid cells. The cell pressure can then be obtained from those of the two materials as an average weighted by the fractional volumes, $f_{i,j}^{(\alpha)}$, of each.

With the fractional volumes, $f_{i,j}^{(\alpha)}$, of the two fluids in the

interface cells known, a simple procedure for obtaining the interface position can be prescribed provided the slope of this boundary does not vary rapidly from cell to cell. If this latter condition is not met, the mesh is probably too coarse to provide an accurate calculation in any event. This procedure, which will be described below by an example, can be used in Cartesian coordinates or in cylindrical coordinates away from the symmetry axis. Consider the situation illustrated below:



We want to calculate the intercept distances $y\Delta y$ on the right of cell (i, j) . It is assumed that the cell types, i.e., the sides cut by the interface in each cell, have already been determined by testing the composition of neighboring cells. A "distance" y can be obtained in three different ways by the assumptions:

- (1) the interface in cell $(i-1, j-1)$ and $(i-1, j)$ is a single straight line
- (2) the interface in cell $(i-1, j)$ and (i, j) is a single straight line
- (3) the interface in cell (i, j) and $(i+1, j)$ is a single straight line

Under the first assumption one obtains the equations,

$$f_{i-1, j-1}^{(2)} = \frac{1}{2} ab$$

$$f_{i-1, j}^{(1)} = \frac{1}{2} y_1 (1-b)$$

$$\frac{a}{b} = \frac{y_1}{1 - b}$$

Therefore

$$y_1 = 2 \left[f_{i-1,j}^{(1)} + \sqrt{f_{i-1,j}^{(1)} f_{i-1,j-1}^{(2)}} \right]$$

Similarly under assumptions (2) and (3) one gets

$$y_2 = 2 \left[\sqrt{f_{i-1,j}^{(1)} [f_{i-1,j}^{(1)} + f_{i,j}^{(1)}]} - f_{i-1,j}^{(1)} \right]$$

$$y_3 = \frac{1}{2} \left[3 f_{i,j}^{(1)} - f_{i+1,j}^{(1)} \right]$$

A simple average of these three quantities will generally give an adequate approximate value for the intercept distance y . Under some circumstances the fractional volumes $f_{i,j}$ may not be compatible with reasonable straight line interfaces through a pair of cells. If this is the case, the final value for the boundary position may be negative or greater than 1. If this should happen, a cruder approximation for y above can be used which is not subject to this type of error. This approximation is to make the boundary position equal to half the sum of the fractional volumes of the two adjacent cells whose common side is cut by the interface. For instance in the above example, set

$$y = \frac{1}{2} \left[f_{i-1,j}^{(1)} + f_{i,j}^{(1)} \right]$$

After the computation of the intersections of the cell boundaries with the fluid interface, which gives the areas (in Cartesian coordinates) available for flow in bi-fluid cells, the cycle of calculation is completed.

Appendix I contains a table of equations for interface positions for different material configurations under the assumption that the boundary though two adjacent cells is a single straight line.

IV. CALCULATIONS OF SUPERSONIC FLOW PAST BLUNT CYLINDRICAL OBSTACLES

As an illustration of the numerical procedures described above and a check on their accuracy, a code for the IBM 7090 digital computer was written to calculate the flow past arbitrarily shaped cylindrical objects. This is a problem which is not generally amenable to direct analytic calculations and is of some intrinsic interest.

Because of the assumed axial symmetry of the obstacles, cylindrical coordinates have been used for this calculation requiring several modifications of the one fluid Eulerian difference equations discussed in Section II. These changes are due to the increase of volume and effective boundary area of a cell as its distance from the axis increases. Equations referring strictly to motion in the axial direction (z-direction) are identical to the Cartesian equations.

If i and j are the cell indices referring to the z and r directions, respectively, and if $j = 1$ gives the row closest to the symmetry axis, the complete set of difference equations for non-fractional cells in cylindrical coordinates is as follows:

Phase I

radial velocity

$$\tilde{u}_{i,j}^{(n)} = u_{i,j}^{(n)} - \frac{p_{i,j+\frac{1}{2}}^{(n)} - p_{i,j-\frac{1}{2}}^{(n)}}{\Delta r} \frac{\Delta t}{\rho_{i,j}^{(n)}}$$

longitudinal velocity

$$\tilde{v}_{i,j}^{(n)} = v_{i,j}^{(n)} - \frac{p_{i+\frac{1}{2},j}^{(n)} - p_{i-\frac{1}{2},j}^{(n)}}{\Delta z} \frac{\Delta t}{\rho_{i,j}^{(n)}}$$

specific energy

$$\begin{aligned} \tilde{E}_{i,j}^{(n)} = E_{i,j}^{(n)} - & \left[\frac{j p_{i,j+\frac{1}{2}}^{(n)} u_{i,j+\frac{1}{2}}^{(n)} - (j-1) p_{i,j-\frac{1}{2}}^{(n)} u_{i,j-\frac{1}{2}}^{(n)}}{(j - \frac{1}{2}) \Delta r} \right. \\ & \left. + \frac{p_{i+\frac{1}{2},j}^{(n)} v_{i+\frac{1}{2},j}^{(n)} - p_{i-\frac{1}{2},j}^{(n)} v_{i-\frac{1}{2},j}^{(n)}}{\Delta z} \right] \frac{\Delta t}{\rho_{i,j}^{(n)}} \end{aligned}$$

where

$$p_{i+\frac{1}{2},j}^{(n)} = \frac{1}{2} [p_{i,j}^{(n)} + p_{i+1,j}^{(n)}], \text{ etc.}$$

Phase II

$$\Delta M_{i-\frac{1}{2},j}^{(n)} = (j - \frac{1}{2}) \rho_{i-\frac{1}{2},j}^{(n)} \tilde{v}_{i-\frac{1}{2},j}^{(n)} \Delta r^2 \Delta t$$

$$\Delta M_{i+\frac{1}{2},j}^{(n)} = (j - \frac{1}{2}) \rho_{i+\frac{1}{2},j}^{(n)} \tilde{v}_{i+\frac{1}{2},j}^{(n)} \Delta r^2 \Delta t$$

$$\Delta M_{i,j-\frac{1}{2}}^{(n)} = (j - 1) \rho_{i,j-\frac{1}{2}}^{(n)} \tilde{u}_{i,j-\frac{1}{2}}^{(n)} \Delta r \Delta z \Delta t$$

$$\Delta M_{i,j+\frac{1}{2}}^{(n)} = j \rho_{i,j+\frac{1}{2}}^{(n)} \tilde{u}_{i,j+\frac{1}{2}}^{(n)} \Delta r \Delta z \Delta t$$

where the $\rho_{i-\frac{1}{2},j}^{(n)}$, $\tilde{v}_{i-\frac{1}{2},j}^{(n)}$, etc. are calculated as in Section II.

Phase III

$$\begin{aligned}
 \rho_{i,j}^{(n+1)} &= \rho_{i,j}^{(n)} + \frac{1}{(j-\frac{1}{2})\Delta r \Delta z} \left[\Delta M_{i-\frac{1}{2},j}^{(n)} - \Delta M_{i+\frac{1}{2},j}^{(n)} \right. \\
 &\quad \left. + \Delta M_{i,j-\frac{1}{2}}^{(n)} - \Delta M_{i,j+\frac{1}{2}}^{(n)} \right] \\
 X_{i,j}^{(n+1)} &= \left(C_{i,j}(1) \tilde{X}_{i-\frac{1}{2},j}^{(n)} \Delta M_{i-\frac{1}{2},j}^{(n)} + C_{i,j}(2) \tilde{X}_{i,j-1}^{(n)} \Delta M_{i,j-\frac{1}{2}}^{(n)} \right. \\
 &\quad \left. + C_{i,j}(3) \tilde{X}_{i+1,j}^{(n)} \Delta M_{i+\frac{1}{2},j}^{(n)} \right. \\
 &\quad \left. + C_{i,j}(4) \tilde{X}_{i,j+\frac{1}{2}}^{(n)} + \tilde{X}_{i,j}^{(n)} \left\{ (j-\frac{1}{2}) \Delta r^2 \Delta z \rho_{i,j}^{(n)} - [1-C_{i,j}(1)] \Delta M_{i-\frac{1}{2},j}^{(n)} \right. \right. \\
 &\quad \left. - [1-C_{i,j}(2)] \Delta M_{i,j-\frac{1}{2}}^{(n)} - [1-C_{i,j}(3)] \Delta M_{i+\frac{1}{2},j}^{(n)} \right. \\
 &\quad \left. \left. - [1-C_{i,j}(4)] \Delta M_{i,j+\frac{1}{2}}^{(n)} \right\} \right) / \left[(j-\frac{1}{2}) \Delta r^2 \Delta z \rho_{i,j}^{(n+1)} \right]
 \end{aligned}$$

where X is u , v , or E ; and $C_{i,j}(k)$ is one or zero depending on whether fluid is flowing into or out of cell (i,j) across side k as defined in Section II.

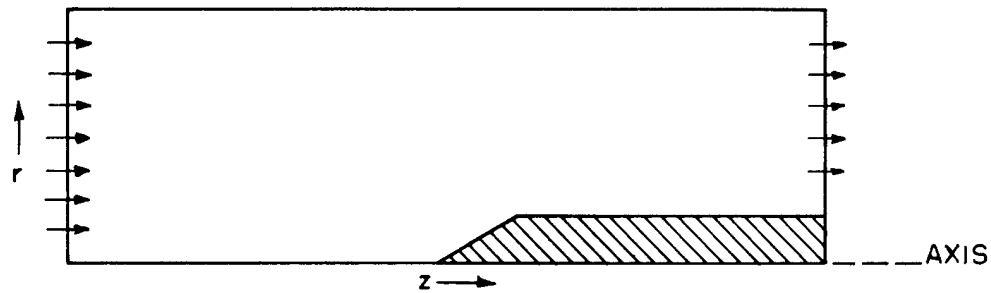
The differences between the Cartesian and cylindrical equations are seen to be minor. Explicit artificial viscosities can be calculated as explained earlier and the rules for treating fractional cells apply unchanged except for the form of the fractional volumes and areas. Appendix II contains a table of fractional areas and volumes for the different types of fractional cells in cylindrical coordinates. One additional difference that should be noted is the boundary condition at the axis of

symmetry. This must be treated as a rigid barrier.

The problems which were run with the obstacle code were chosen to coincide with a set of supersonic wind tunnel experiments by Marschner² and a similar experiment at a higher Mach number by Oguchi.³ The Marschner experiments which were simulated were the flow of air past a right circular cylinder at Mach 1.58 and the flow of air past a cone of 75° vertex angle attached to a circular cylinder, at Mach numbers 1.41, 1.58, and 1.71. The Mach 1.41 case was also rerun at double the mesh resolution in order to obtain an idea of gain in accuracy which could be brought about by decreasing the cell size. The experiment of Oguchi which was considered was again the flow of air past a right circular cylinder but at Mach 4.3. In all of these experiments, a detached shock wave was present. The data on the flows which were available and with which the machine computations were compared were the positions of the shock fronts and the pressure distributions at the obstacle. Oguchi's results also provide the position of the sonic line — line of Mach 1 — and the stream line pattern immediately beyond the shock.

The hydrodynamic differencing scheme which was described in the previous sections is explicitly a method for time dependent problems. For stationary problems it is necessary to begin the calculation with an arbitrary configuration of the fluid, always keeping the correct boundary conditions, and advance the time until a steady state is reached. Thus the computation contains the dynamics of the approach to steady state as well as the steady-state flow itself. In the present calculations a rectangular mesh was set up as shown with the axis of symmetry as the

bottom boundary. The upper boundary was assumed rigid.



Fluid entered at the left with the free stream conditions

$$\rho_0 = 1, \quad u_0 = 0, \quad c_0 = \text{sound speed} = 1,$$

$$v_0 = M_0 = \text{Mach number}$$

and excited at the right. The equation of state was that for a polytropic gas with $\gamma = 1.4$.

$$p = (\gamma - 1) \rho [E - \frac{1}{2} (u^2 + v^2)]$$

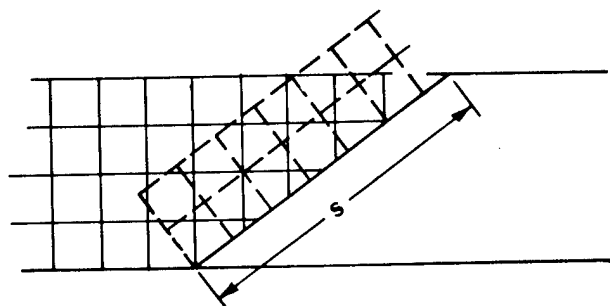
The initial fluid parameters throughout the mesh were chosen equal to the free stream parameters. These initial conditions correspond to the impulsive start up of the obstacle in a stationary medium as seen from a reference frame in which the obstacle is at rest. In the case of the cone tipped cylinders, velocities throughout the mesh were sufficiently high that the use of an explicit viscous pressure was not considered essential. Such a term was used, however, with the blunt nosed (180° cone) cylinders. The following table lists the mesh characteristics and viscous pressure parameters used in the present calculations:

Cone Angle	Mach Number	Mesh Size (r x z)	Obstacle Radius	Viscous Pressure Parameters
75°	1.41	40 x 60 cells	9 cells	none
75°	1.58	40 x 60 cells	9 cells	none
75°	1.71	40 x 60 cells	9 cells	none
75°	1.41	60 x 60 cells	18 cells	none
180°	1.58	44 x 44 cells	14 cells	A = 1.5 B = 0.3
180°	4.3	44 x 44 cells	14 cells	A = 1.5 B = 0.3

The time steps Δt were chosen so that $M \times \Delta t \approx 1/10 \Delta r$. In all cases Δr and Δz were equal. Problems were allowed to run until it was judged that changes in the mesh parameters between a time t and $t + 40 \times \Delta t$ were negligible. These running times were on the order of two to three hours.

In order to compare the results of the machine calculations with the experimental data for each problem, plots were made of the computed position of the detached shocks and of the ratio of the pressure at the surface of the obstacle to the true stagnation pressure. In addition, stream lines for each flow were obtained by following the trajectories of "test particles" through the mesh using the computed steady-state velocities. Linear interpolation between the velocities at the cell centers was used to obtain the test particle velocity. The stream-line plots which follow were made directly from computer results by an automatic plotter and not hand drawn. In the Mach 4.3 case, an additional graph compares the computed and experimental stream lines.

In the case of the blunt cylinders, surface pressures were obtained by a linear extrapolation from the pressures at the centers of the cells immediately in front of the obstacle. A similar procedure was followed for the 75° cones. However there, in an attempt to minimize the effects of fluctuations of pressure in the small fractional cells and to provide a systematic method for extrapolation to the obstacle, two rows of cells were constructed parallel to the surface of the cone as shown below. Pressures



at the centers of the tilted cells were obtained from the pressures within the normal mesh as an average weighted by the area of each normal cell within a slant cell. With these averaged values, the pressures along the cone were obtained by extrapolation. In the graphs, distance along the cone is measured in units of the slant length s as shown. This length is just the radius of the cylinder for the blunt faced obstacles. The solid lines give the experimental curves while the calculated values are shown by circled points connected by broken lines. As mentioned before, pressures were plotted in units of the true stagnation pressure in each case. These stagnation pressures can be obtained by following an element of fluid along the axial stream line. From the extreme left until the shock front, this element flows with the free stream parameters. At the shock

the parameters change discontinuously according to the normal Hugoniot relations to

$$\rho' = \frac{(\gamma+1)\rho_0 M_0^2}{2 + (\gamma-1)M_0^2}, \quad v' = \frac{\rho_0 v_0}{\rho'}, \quad p' = p_0 + \rho_0 v_0 (v_0 - v')$$

From just beyond the shock to the stagnation point, $v = 0$, Bernoulli's law and the adiabatic equation of state may be used to give the stagnation pressure and density. Thus

$$\frac{\gamma}{\gamma-1} \frac{p_s}{\rho_s} = \frac{1}{2} v'^2 + \frac{\gamma}{\gamma-1} \frac{p'}{\rho'}$$

and

$$\frac{p_s}{\rho_s^\gamma} = \frac{p'}{\rho'^\gamma}$$

or

$$p_s = \left[\left(\frac{1}{2} \frac{\gamma-1}{\gamma} v'^2 + \frac{p'}{\rho'} \right) \frac{\rho'}{p'^{1/\gamma}} \right] \frac{\gamma}{\gamma-1}$$

The stagnation pressures for the situations considered are as follows:

Mach Number	Stagnation Pressure
1.41	2.20
1.58	2.66
1.71	3.05
4.3	17.34

Shock fronts were obtained from the calculations by first making plots of density versus axial position for each row of cells in the case of the blunt cylinders and Mach number versus axial position for the 75° cones. These show a steep rise in the vicinity of the shock followed by

a more gradual rise or decline. The plots are given in Appendix III. Because of the smearing of the shock front by the implicit viscous pressure inherent in the calculation, the position of the shock is necessarily subjective to some degree. The shock front lies roughly halfway between the point of the initial steep rise and the point where the rise is judged to terminate in the density or Mach number curve. A set of unconnected points marking the predicted shock position have been plotted in each case as well as a solid line marking the experimental shock front. In addition, a pair of dashed lines obtained from the approximate one quarter and three quarter positions on the calculated shock rise curves have been shown. These define an approximate limiting region in which the predicted shock must lie. In the Mach 4.3 problem, the experimental and theoretical sonic lines are also given. Figures 4 through 22 show the stream lines, shock front, and surface pressure distribution for each of the six problems considered.

An examination of the graphs shows that, in general, reasonably good agreement between theory and experiment can be obtained by the numerical methods employed. The estimated positions of the shock fronts agree with experiment to better than one cell width in all cases except that of the blunt cylinder at Mach 1.58. There the predicted shock lies farther from the obstacle than that determined experimentally, though both curves are similar. The displacement of the calculated shock intercept with the axis of symmetry with respect to the experimental value amounts to about

(Text continues Page 81)

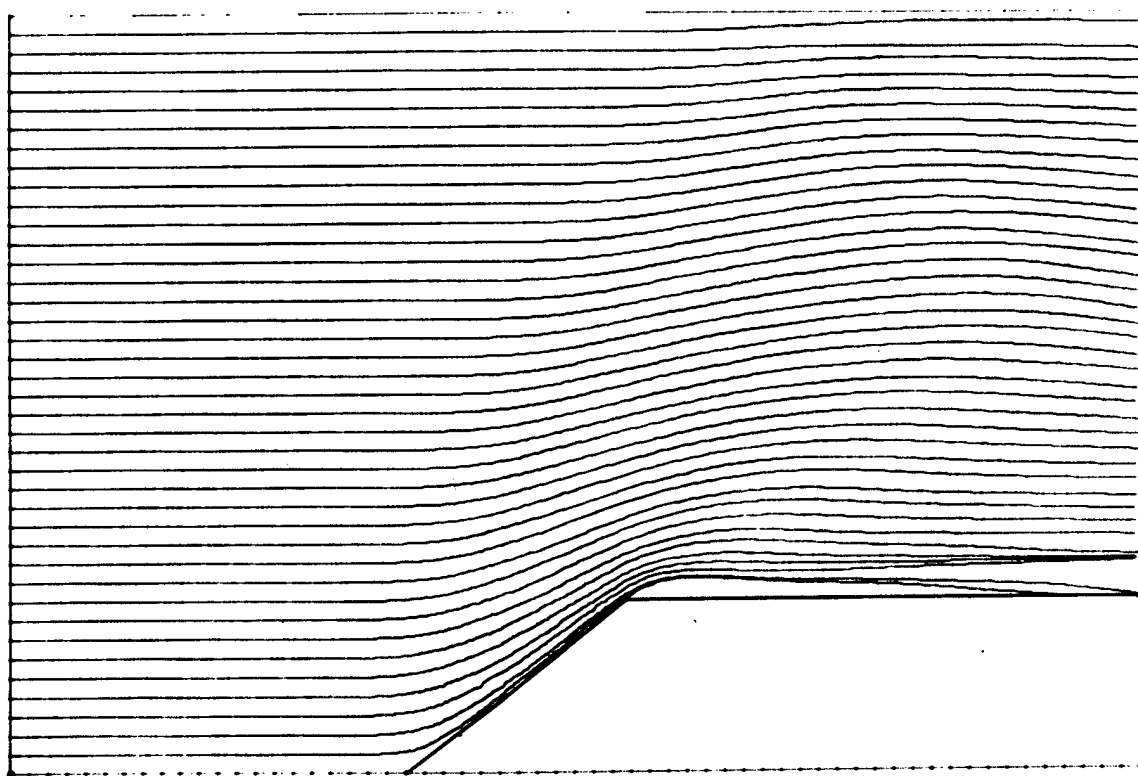


Figure 4. Stream lines, 75° cone. Mach 1.41, 40×60 mesh

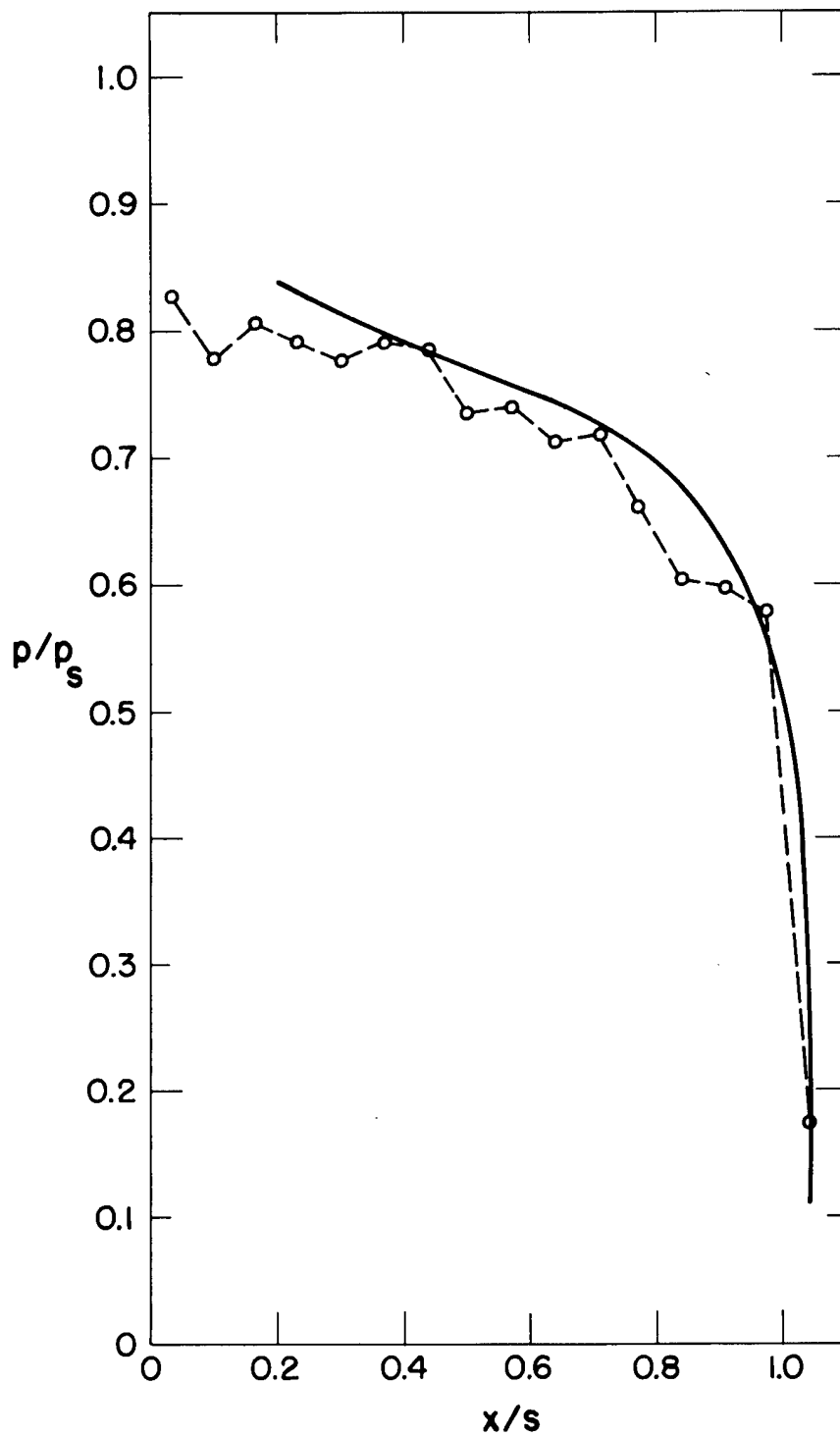


Figure 5. Obstacle pressures, 75° cone. Mach 1.41, 40×60 mesh

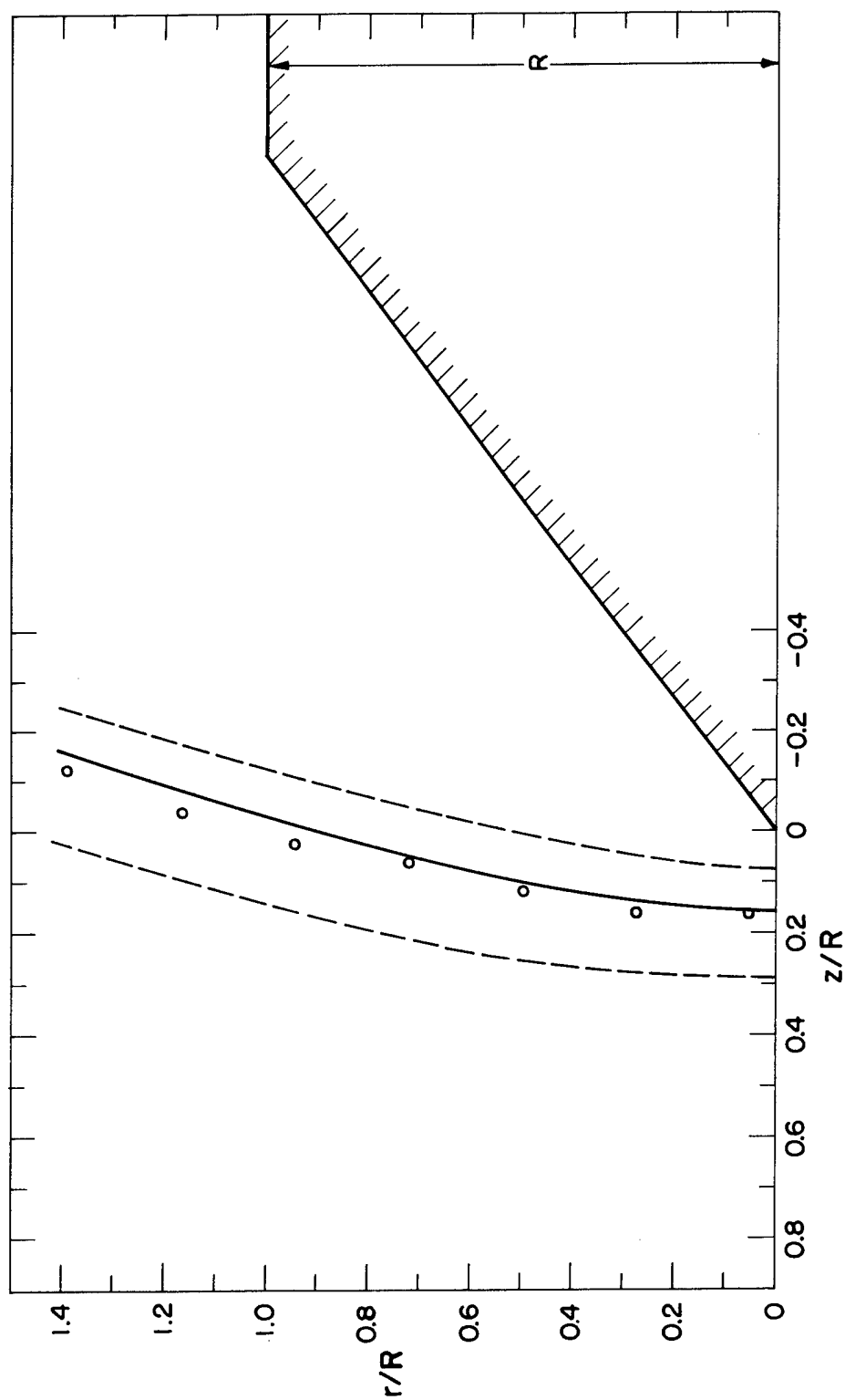


Figure 6. Detached shock position, 75° cone. Mach 1.41, 40 × 60 mesh

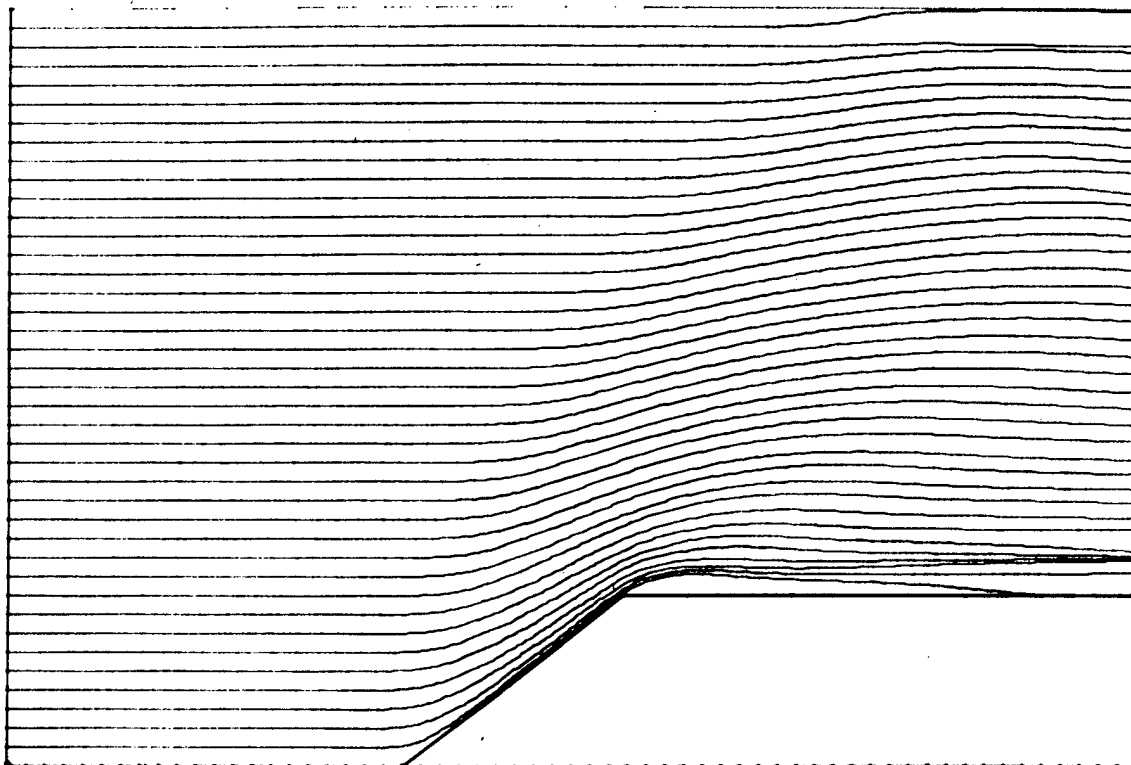


Figure 7. Stream lines, 75° cone. Mach 1.58

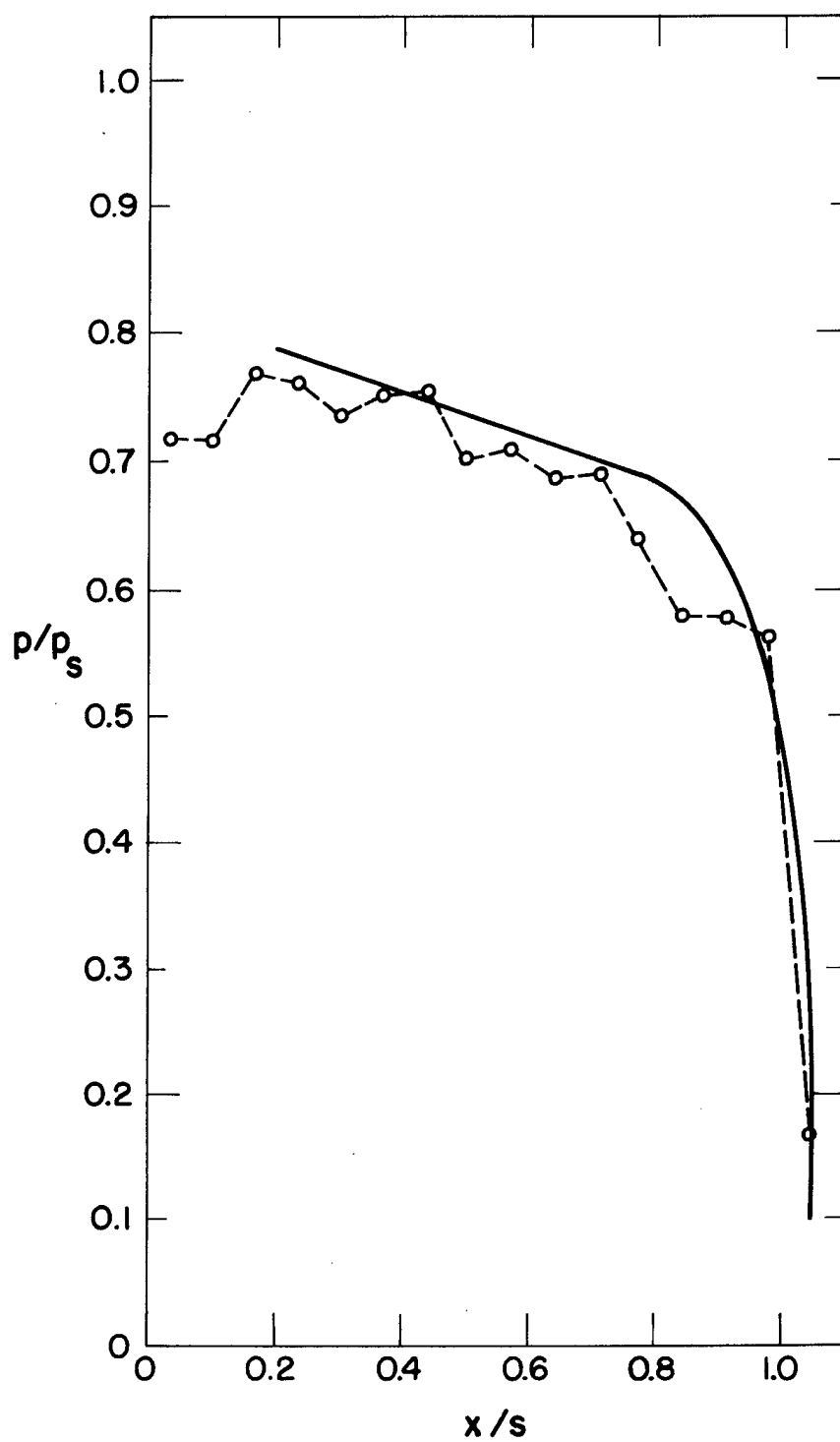


Figure 8. Obstacle pressures, 75° cone. Mach 1.58

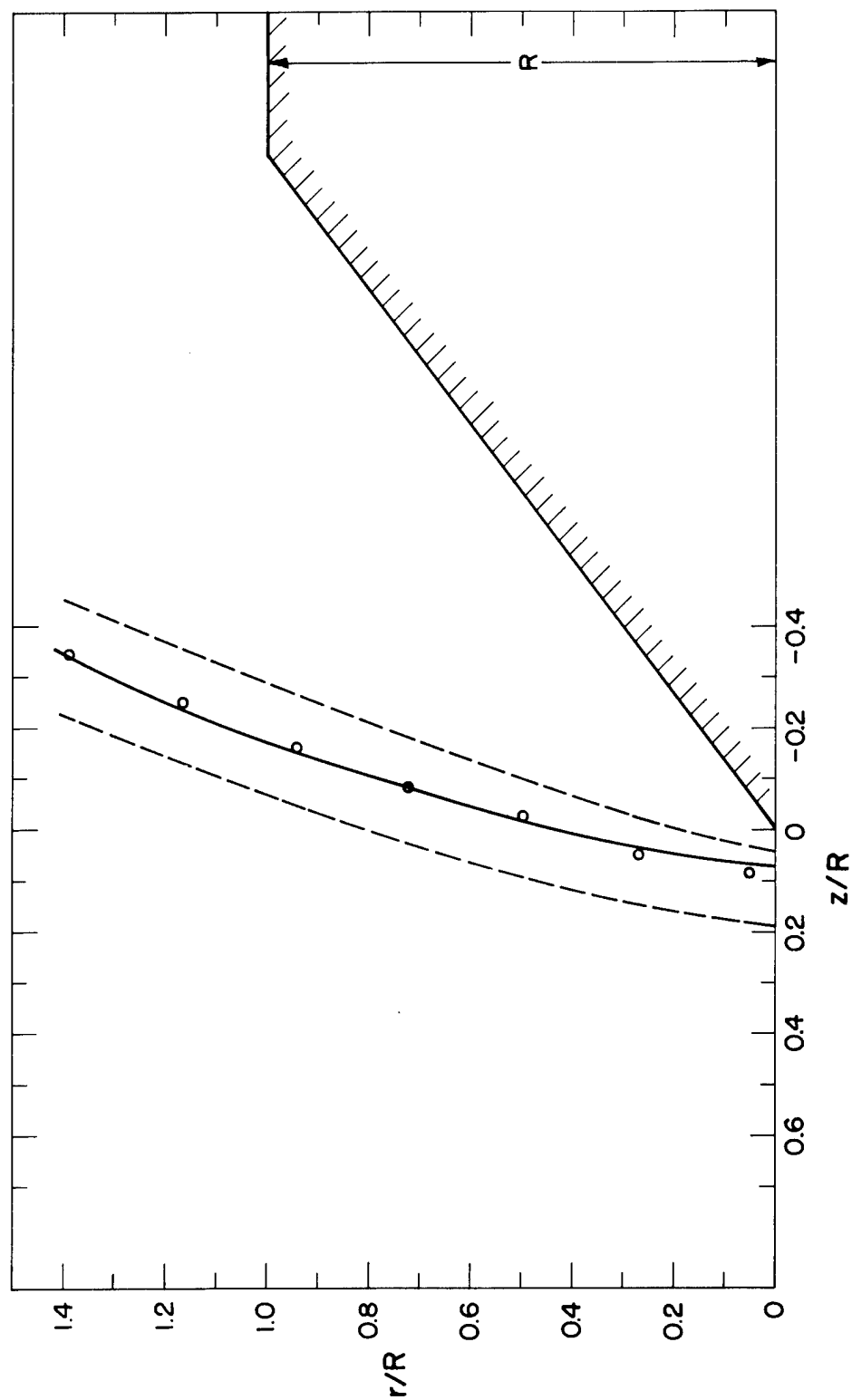


Figure 9. Detached shock position, 75° cone. Mach 1.58

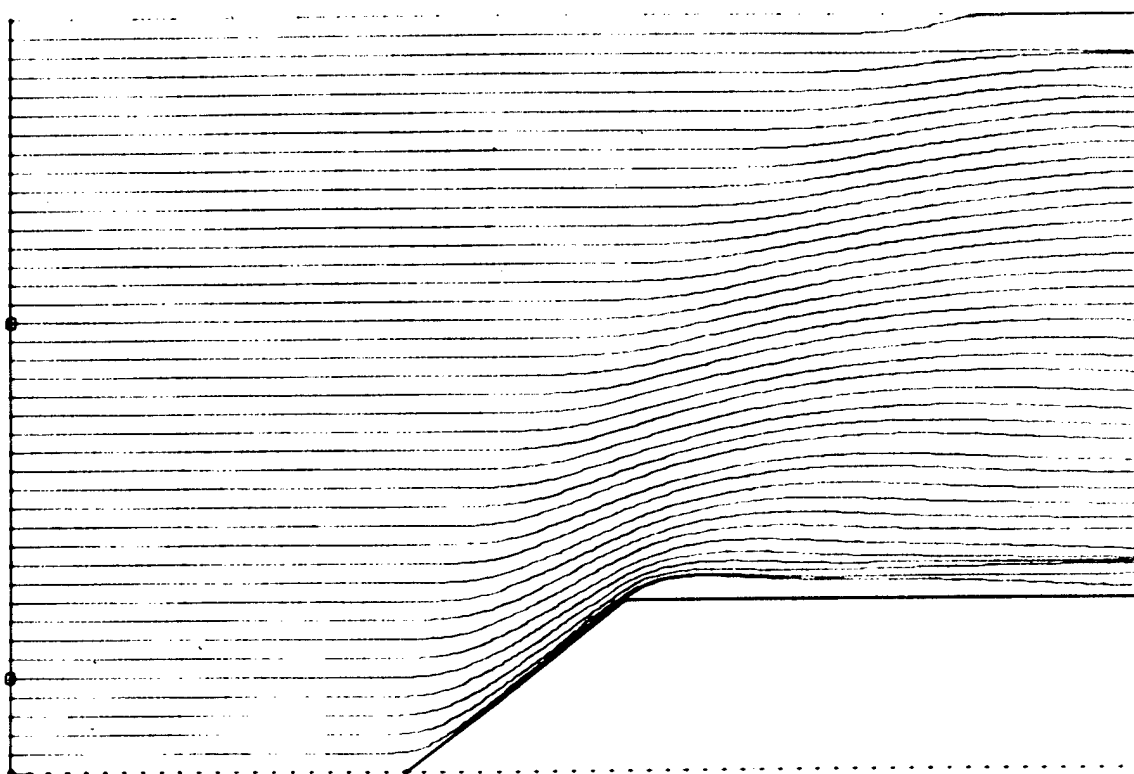


Figure 10. Stream lines, 75° cone. Mach 1.71

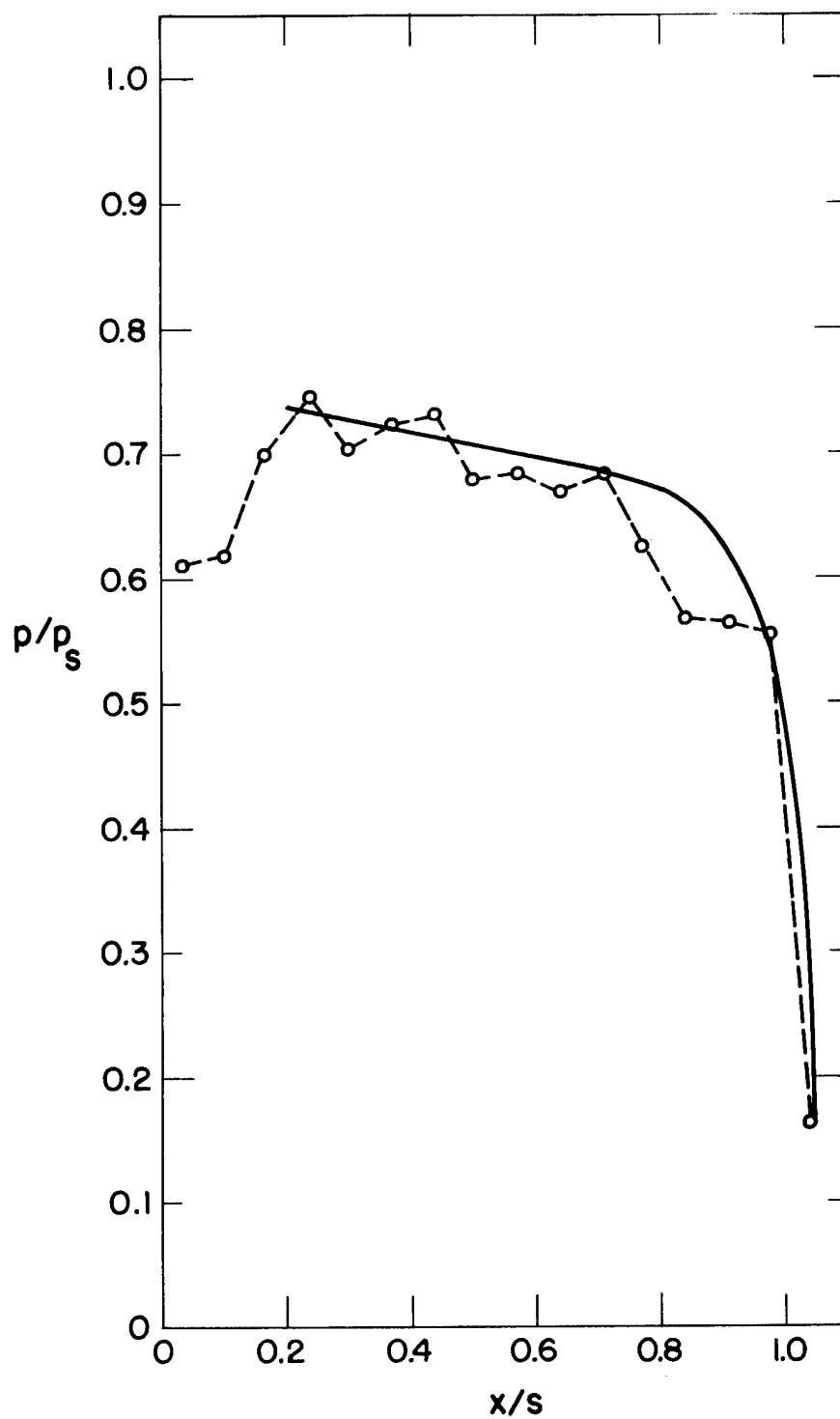


Figure 11. Obstacle pressures, 75° cone. Mach 1.71

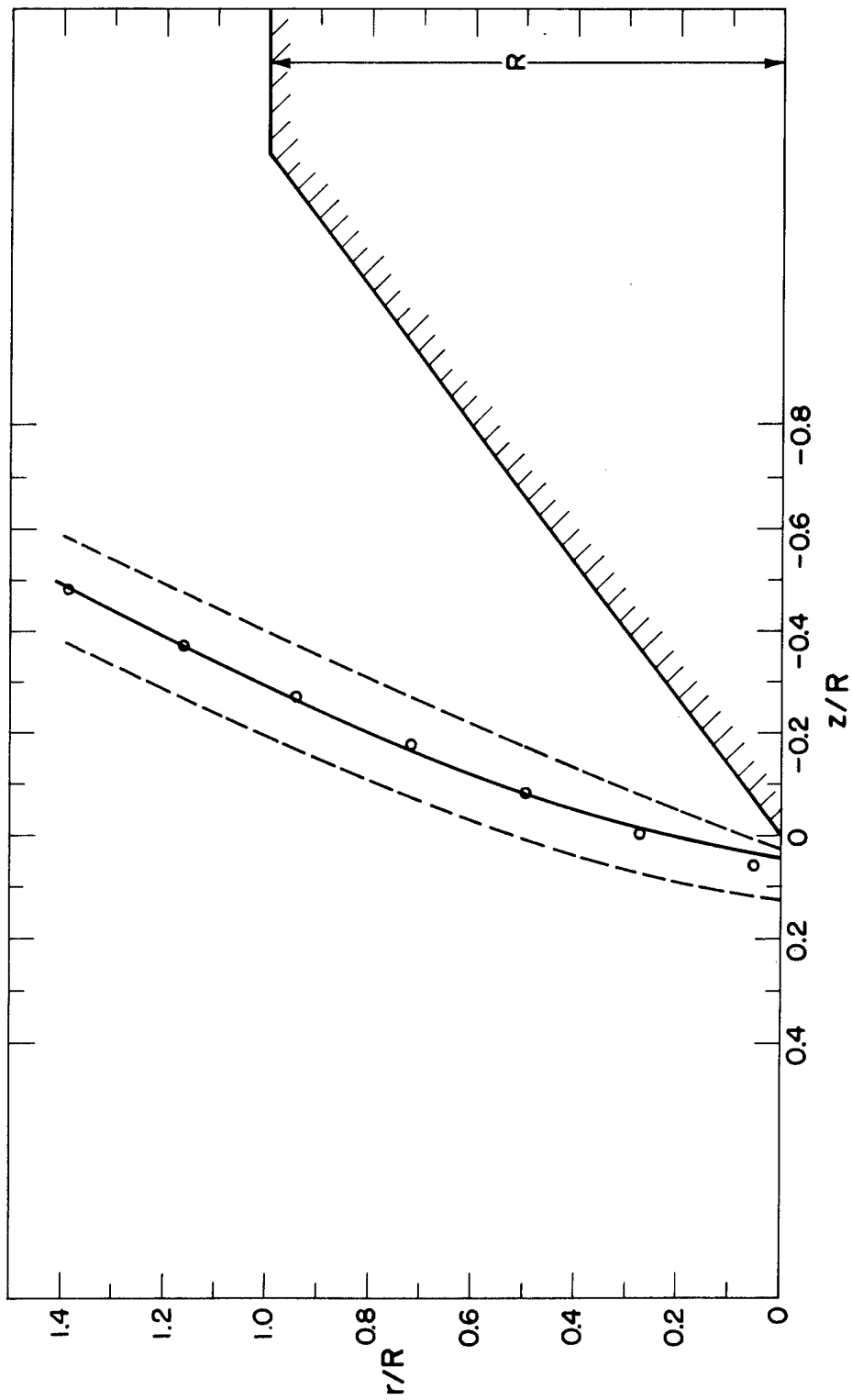


Figure 12. Detached shock position, 75° cone. Mach 1.71

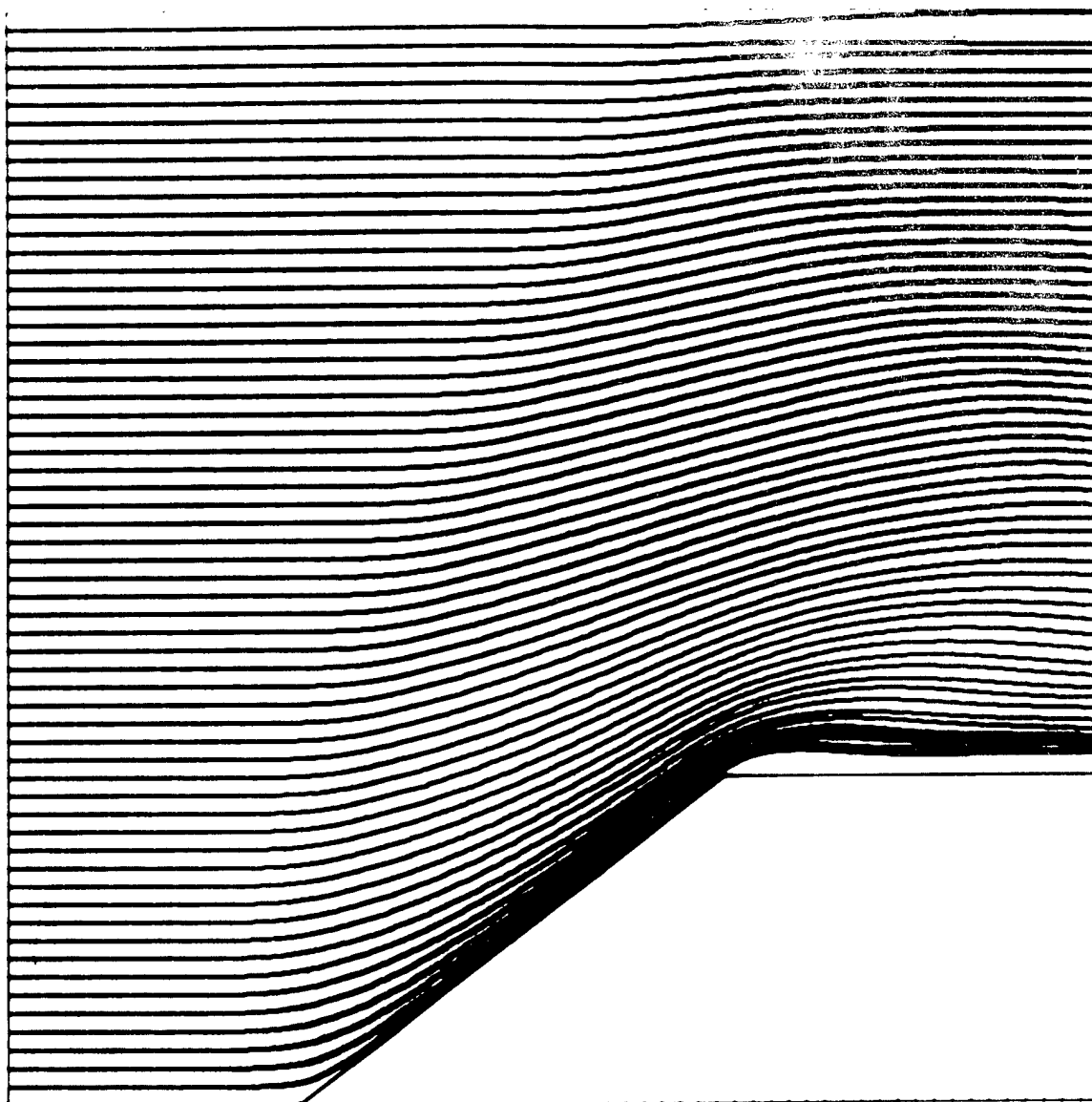


Figure 13. Stream lines, 75° cone. Mach 1.41, 60×60 mesh

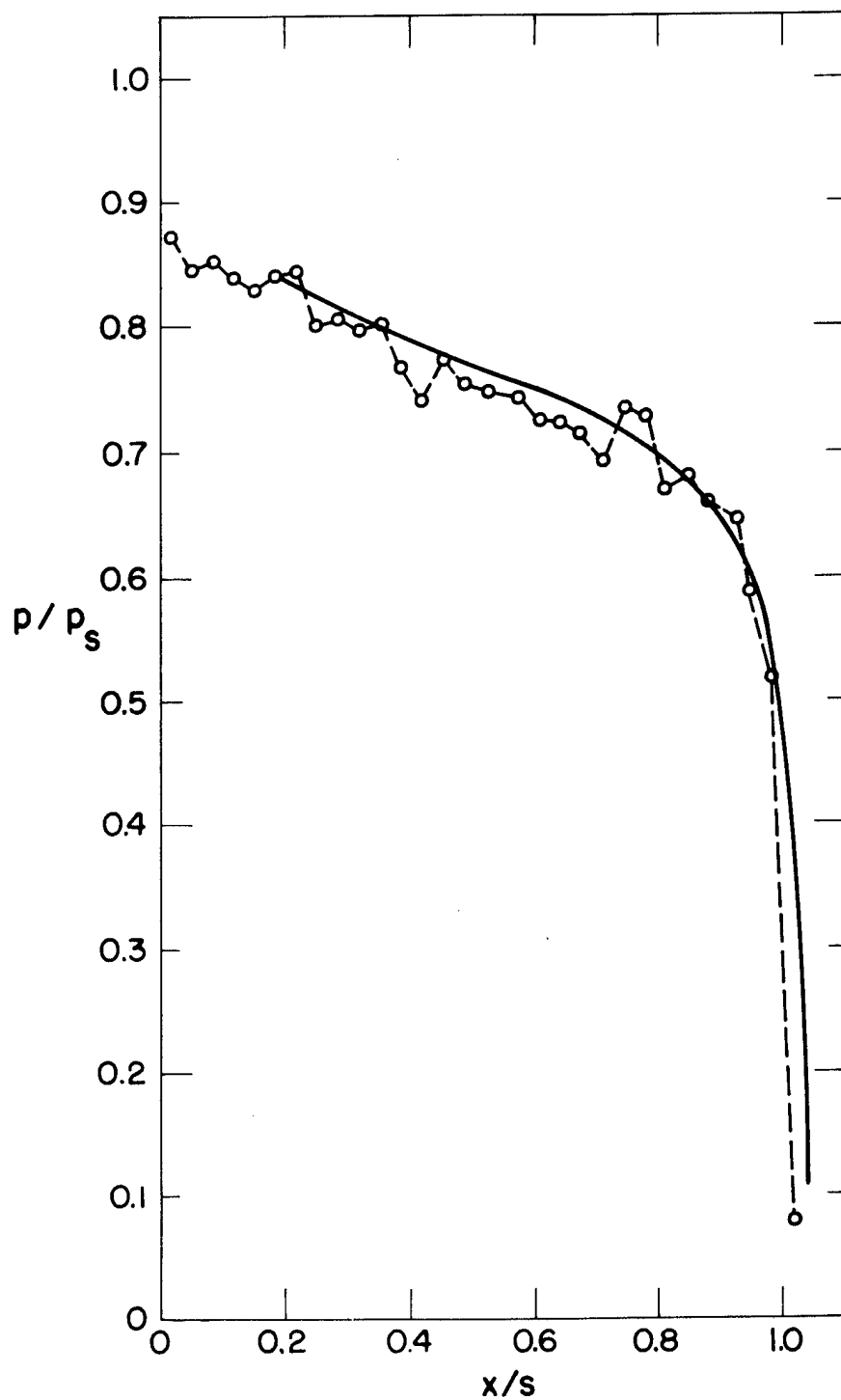


Figure 14. Obstacle pressures, 75° cone. Mach 1.41, 60×60 mesh

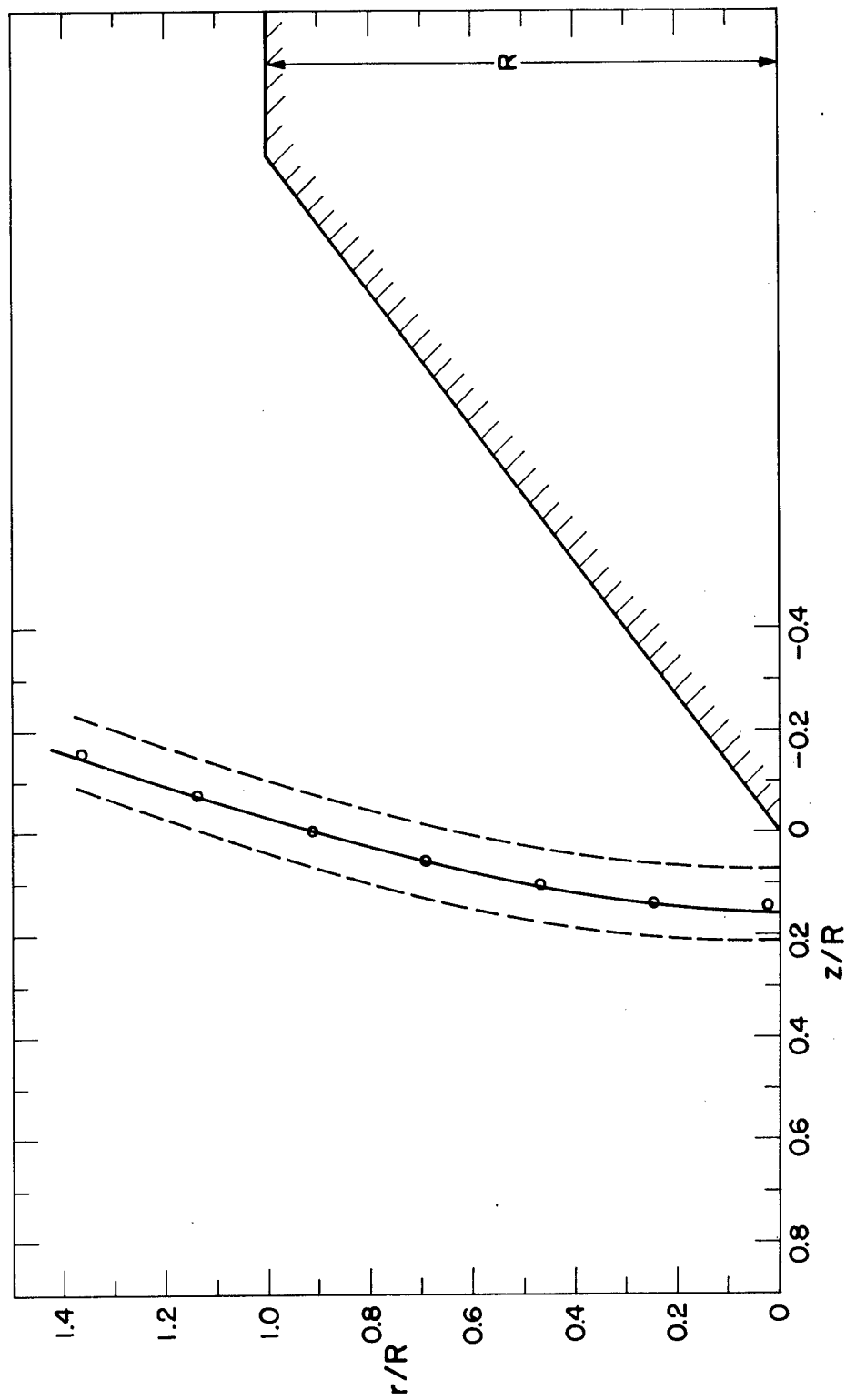


Figure 15. Detached shock position, 75° cone. Mach 1.41, 60 X 60 mesh

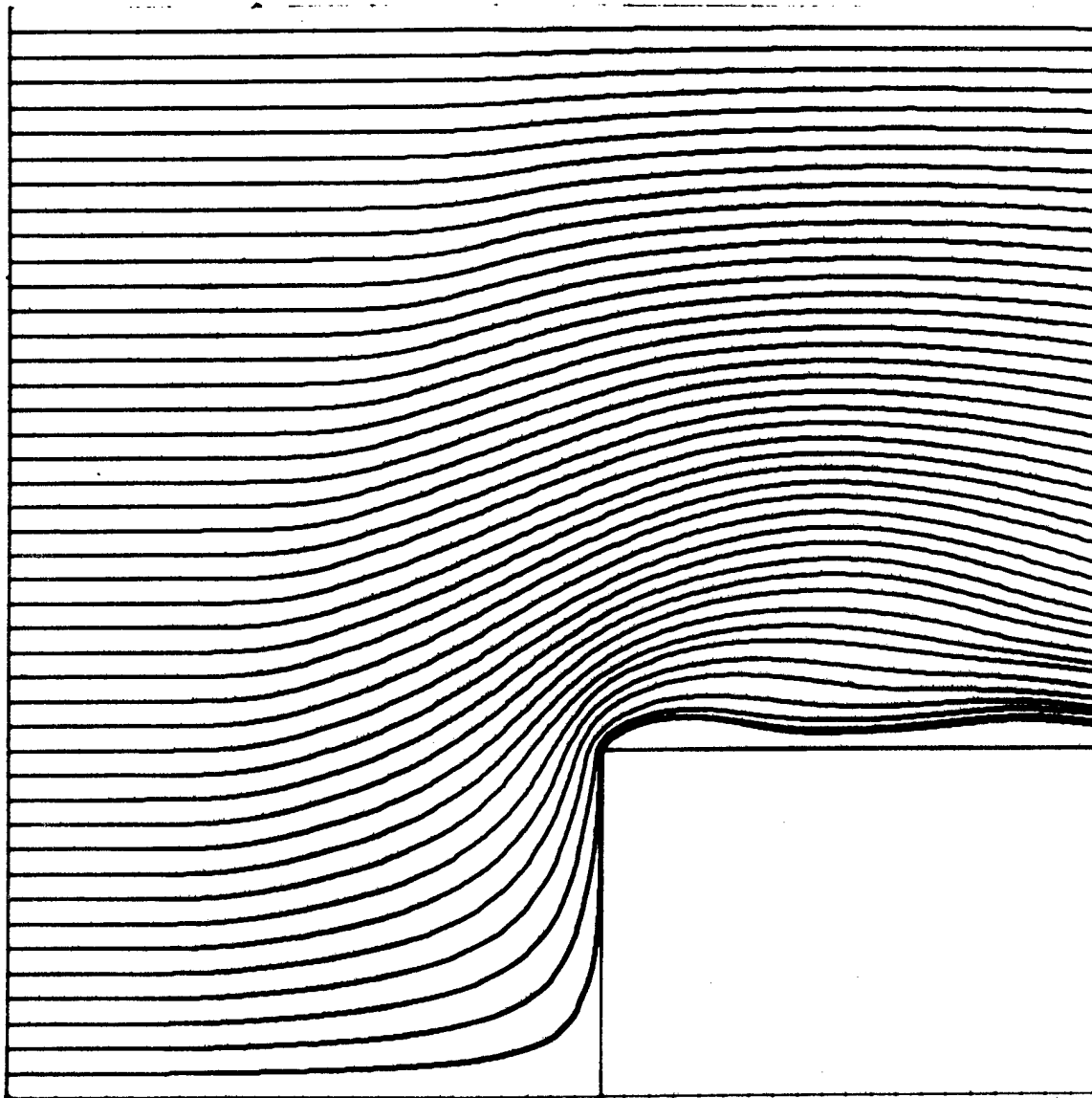


Figure 16. Stream lines, 180° cone. Mach 1.58

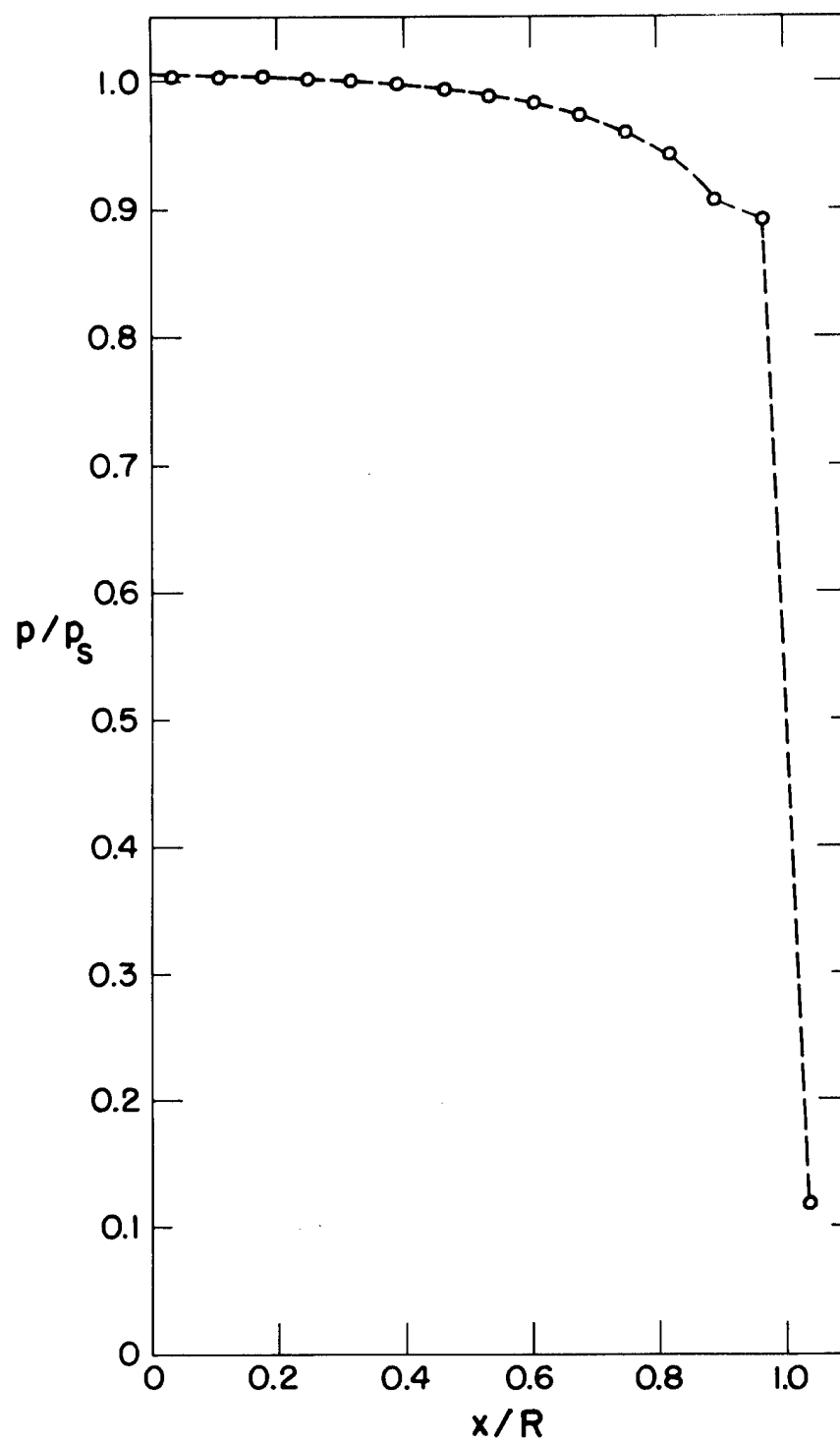


Figure 17. Obstacle pressures, 180° cone. Mach 1.58

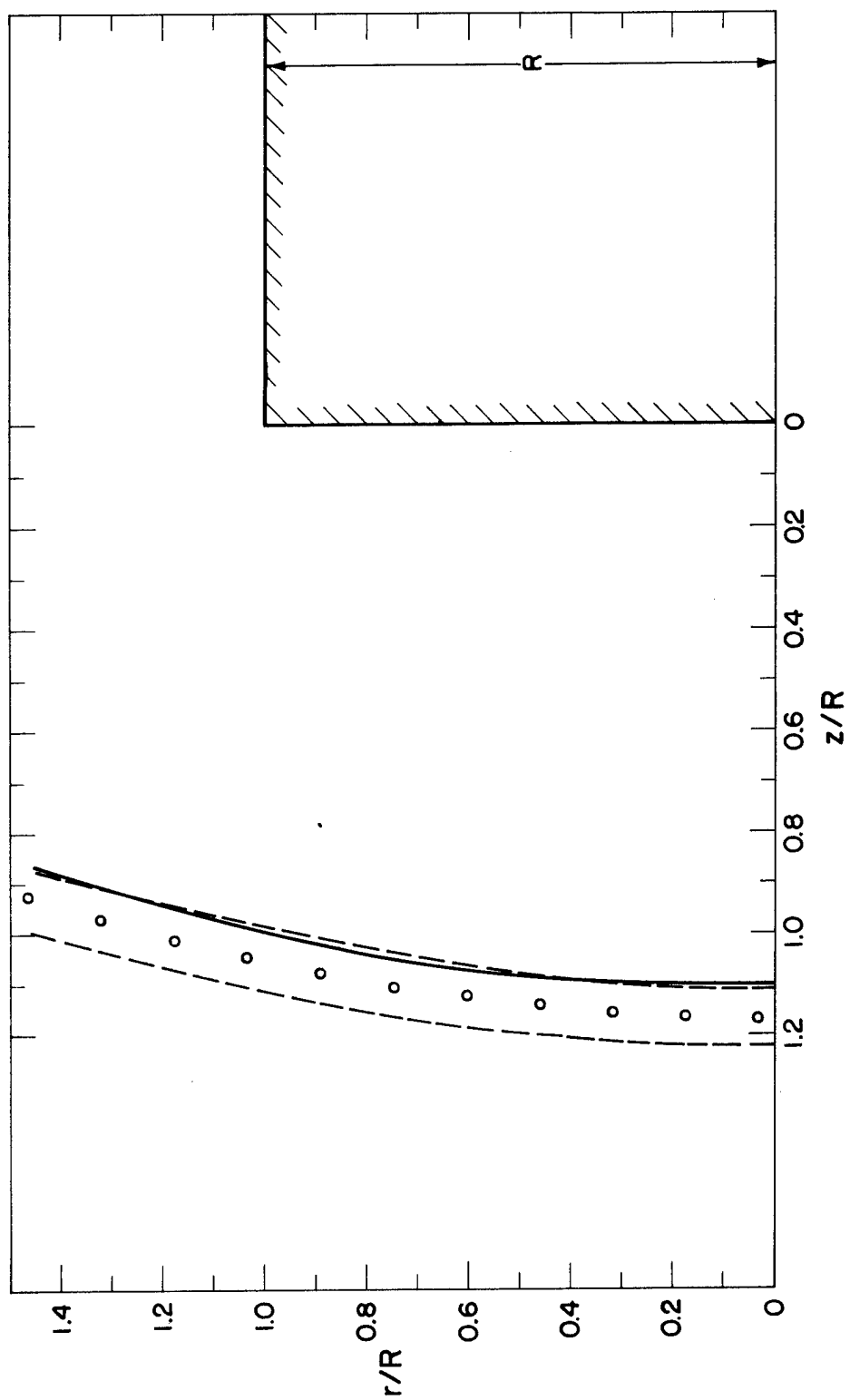


Figure 18. Detached shock position, 180° cone. Mach 1.58

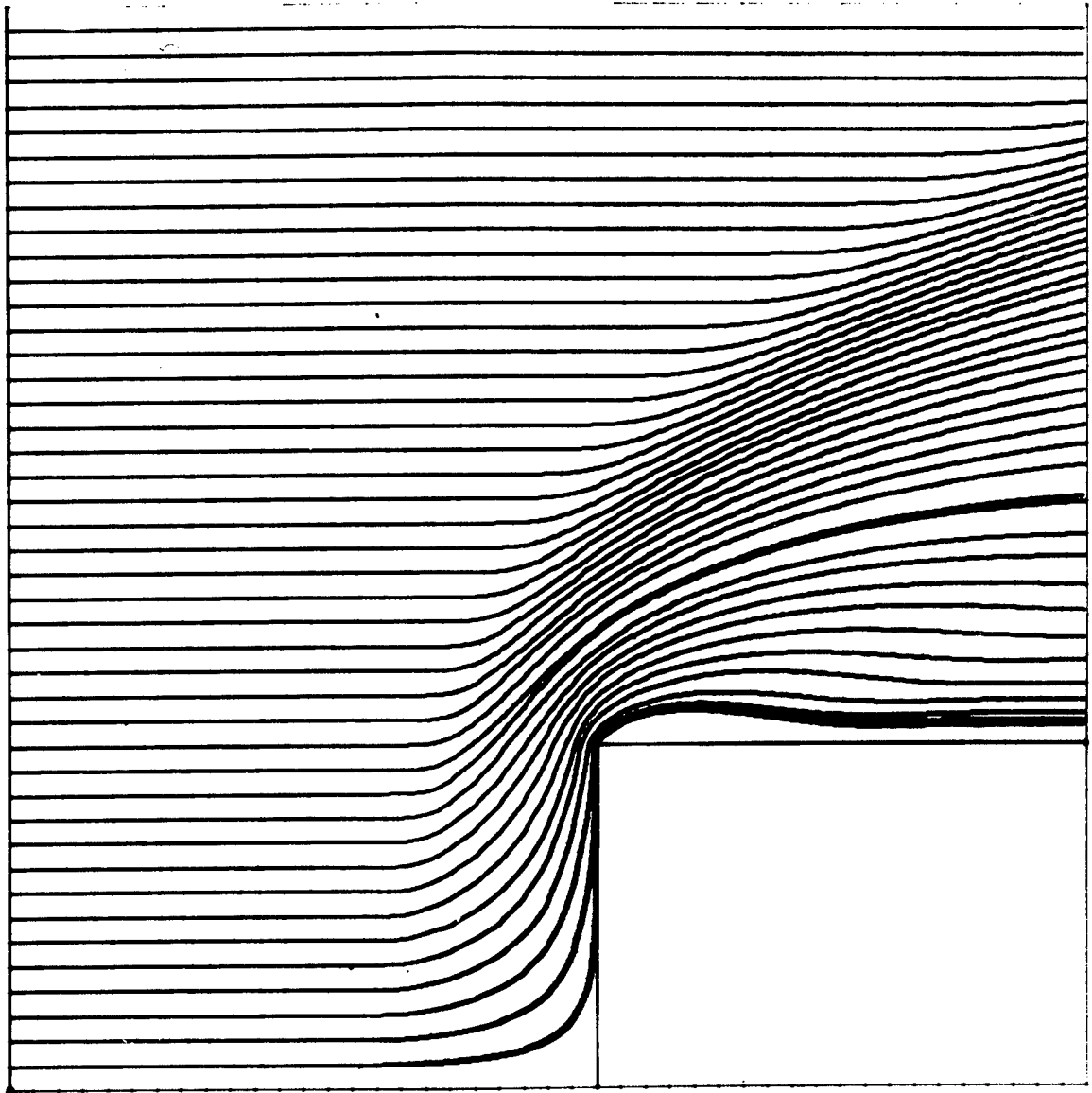


Figure 19. Stream lines, 180° cone. Mach 4.3

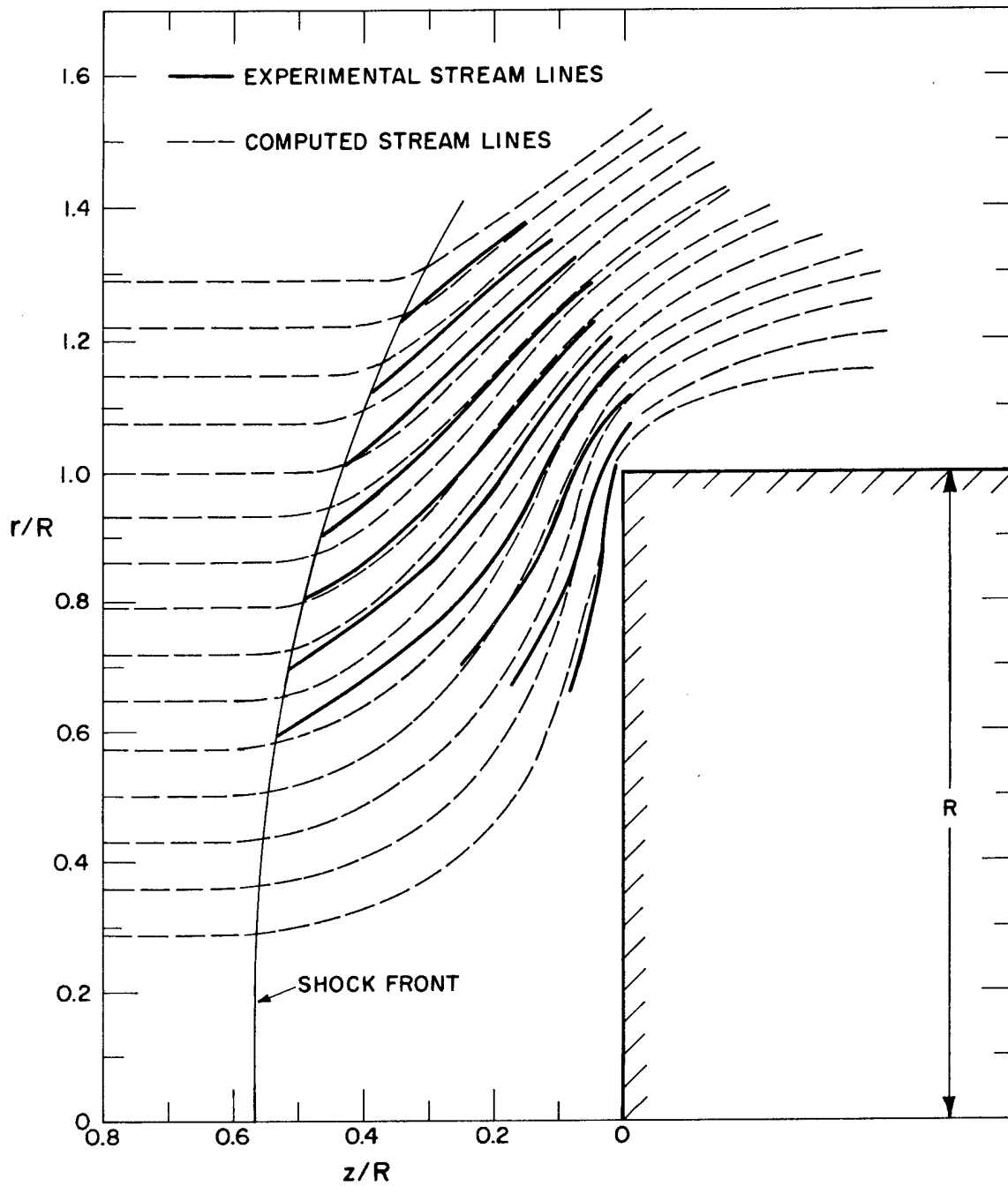


Figure 20. Stream lines, 180° cone. Mach 4.3

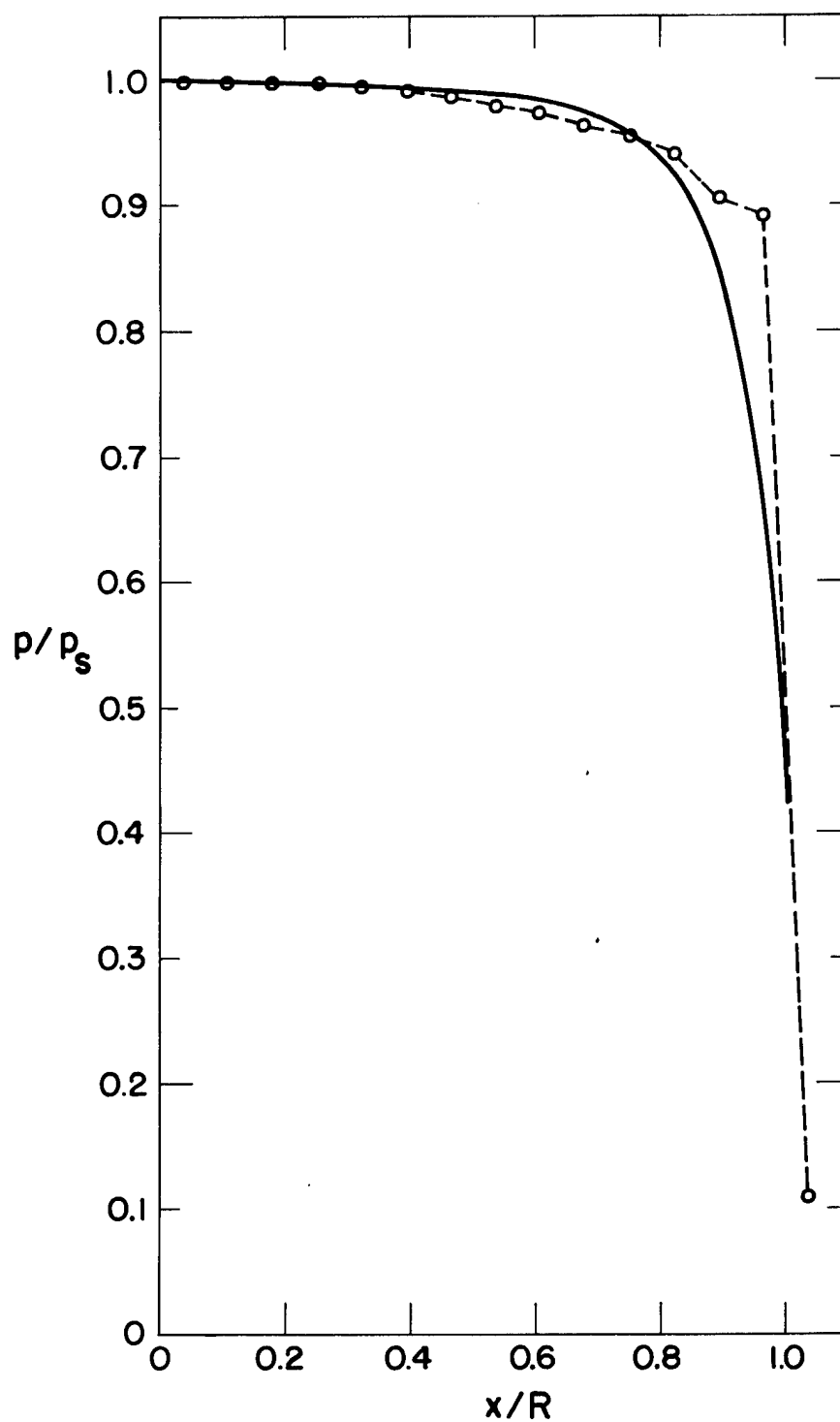


Figure 21. Obstacle pressures, 180° cone. Mach 4.3

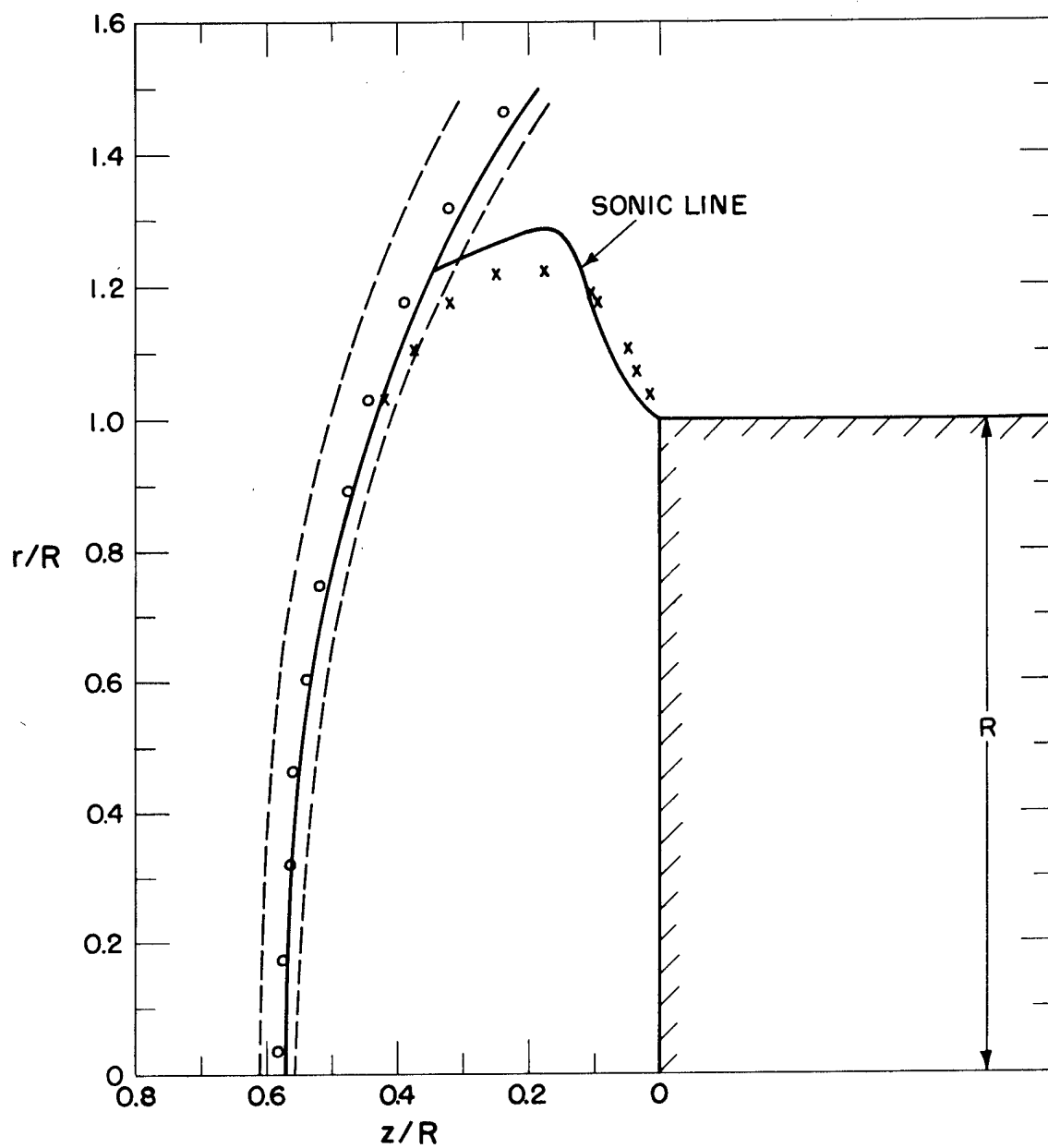


Figure 22. Detached shock position, 180° cone. Mach 4.3

a five percent deviation. The source of this discrepancy is not known, especially since no estimates of experimental errors were given by Marschner.²

The comparison of the calculated and experimental pressure distributions at the obstacle is somewhat marred by the relatively large fluctuations for the 75° cones of nine cell radius. Increasing the resolution of the mesh as was done in the case of the Mach 1.41 cone reduced these fluctuations substantially and resulted in good agreement with experiment. In general, the calculated pressures follow the trend of the experimental pressures at roughly the correct magnitudes. The use of an explicit viscous pressure term in the cone problems would have probably reduced the pressure fluctuations near the obstacle and generally improved the agreement with experiment. For the blunt cylinders, no experimental pressures at Mach 1.58 were available. In the Mach 4.3 problem agreement between calculation and experiment is good except near the shoulder of the cylinder where the calculated pressures are somewhat high.

In conclusion, the present numerical method for solving the hydrodynamic equations for supersonic compressible flows will give adequate results where extreme precision is not required. The accuracy of the scheme depends on the nature of the problem and on specific quantity under consideration as well as on the relative size of the mesh compared to the expected spatial variations of physical quantities, on the time step, and on the proper use of an explicit viscous pressure term. In

the present problems, this accuracy may be estimated at about five percent. There is still much room for improvement in the method. Higher order accuracy could probably be incorporated in the equations without undue difficulty. However, perhaps the most important undertaking would be to improve the treatment of boundary condition, particularly in the case of fractional and multifluid cells.

REFERENCES

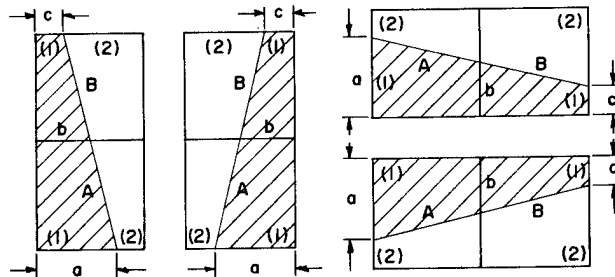
1. Francis H. Harlow and Martha Evans, Los Alamos Scientific Laboratory Report LA-2139 (1957). This is the earliest of a number of reports concerning the PIC method.
2. B. W. Marschner, An Investigation of Detached Shock Waves, Thesis, California Institute of Technology (1948).
3. H. Oguchi, Report No. 341 (1959). Aeronautical Research Institute, University of Tokyo.
4. Courant, Friedrichs, and Lewy, Math. Ann. 100, 32 (1928).
5. J. von Neumann and R. D. Richtmyer, J. Appl. Phys. 21, 232 (1950).
6. R. Landshoff, Los Alamos Scientific Laboratory Report LA-1930 (1955).

APPENDIX I

The following equations give the intercept with the cell boundaries of the interface between a pair of fluids in an Eulerian mesh under the following assumptions:

- a. Cartesian coordinates are appropriate.
- b. The cell dimensions are $\Delta x = \Delta y = 1$.
- c. The fluid interface is a single straight line segment within a pair of adjacent mesh cells.
- d. The fractional areas $f_{i,j}$ occupied by each fluid within a two fluid cell are known. The subscripts (i,j) will be abbreviated by the single capital letters A or B.

1.



$$f_A(1) = \frac{1}{2} (a + b)$$

$$f_B(1) = \frac{1}{2} (b + c)$$

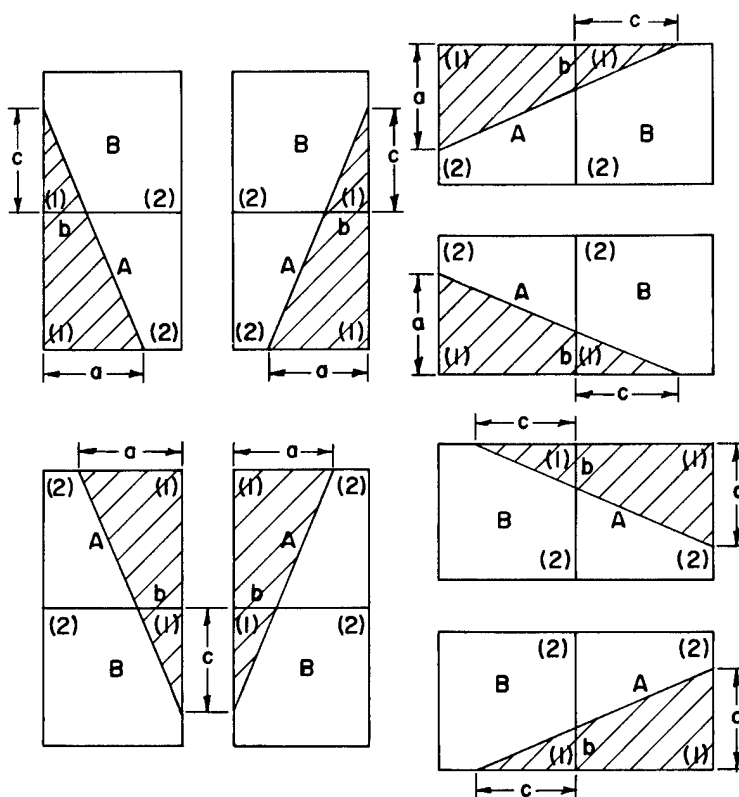
$$b = \frac{1}{2} (a + c)$$

$$\therefore a = 2 f_A(1) - b = \frac{3}{2} f_A(1) - \frac{1}{2} f_B(1)$$

$$b = \frac{1}{2} [f_A(1) + f_B(1)]$$

$$c = 2 f_B(1) - b = \frac{3}{2} f_B(1) - \frac{1}{2} f_A(1)$$

2.



$$f_A(1) = \frac{1}{2} (a + b)$$

$$f_B(1) = \frac{1}{2} b c$$

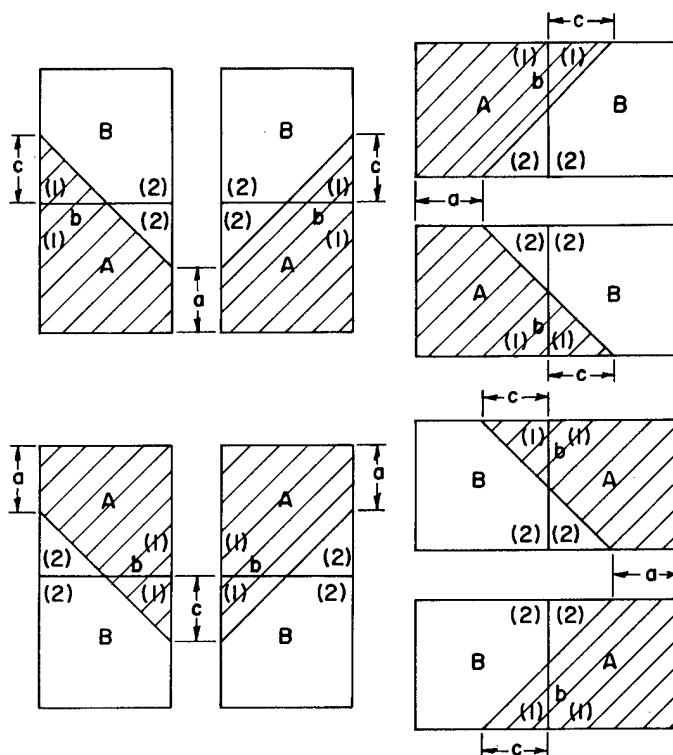
$$\frac{c}{b} = \frac{1}{a - b}$$

$$a = 2 f_A(1) - b = 2 \left\{ f_A(1) + f_B(1) - \sqrt{f_B(1) [f_B(1) + f_A(1)]} \right\}$$

$$b = 2 \left\{ \sqrt{f_B(1) [f_B(1) + f_A(1)]} - f_B(1) \right\}$$

$$c = \frac{2 f_B(1)}{b} = \frac{f_B(1)}{\sqrt{f_B(1) [f_B(1) + f_A(1)]} - f_B(1)}$$

3.



$$f_A(1) = 1 - \frac{1}{2} (1 - a) (1 - b)$$

$$f_B(1) = \frac{1}{2} b c$$

$$\frac{b}{c} = \frac{(1 - b)}{(1 - a)}$$

$$a = 1 - \frac{2[1 - f_A(1)]}{1 - b} = 1 - 2 \left\{ 1 - f_A(1) + \sqrt{[1 - f_A(1)] f_B(1)} \right\}$$

$$b = \frac{1}{1 + \sqrt{[1 - f_A(1)]/f_B(1)}}$$

$$c = \frac{2 f_B(1)}{b} = 2 \left\{ f_B(1) + \sqrt{[1 - f_A(1)] f_B(1)} \right\}$$

APPENDIX II

The following equations give the fractional areas, A_k , and fractional volumes, f , available to a fluid in a mesh cell partially occupied by a rigid obstacle in cylindrical coordinates. It is assumed that $\Delta r = \Delta z = 1$ and that the left- and right-hand cell sides will be designated by subscripts 1 and 3, and the bottom and top sides by 2 and 4, respectively.

1.

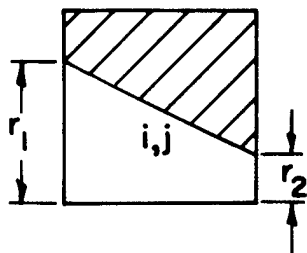
$$A_1 = \frac{r_1(j-1 + \frac{1}{2} r_1)}{j - \frac{1}{2}}$$

$$A_2 = 1$$

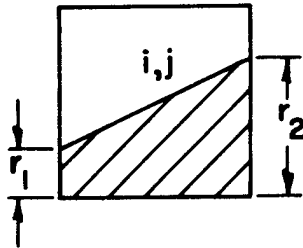
$$A_3 = \frac{r_2(j-1 + \frac{1}{2} r_2)}{j - \frac{1}{2}}$$

$$A_4 = 0$$

$$f_{i,j} = \frac{(j-1)(r_1+r_2) + r_1 r_2 + 1/3 (r_2-r_1)^2}{2j-1}$$



2.



$$A_1 = \frac{\left(j - \frac{1-r_1}{2}\right)(1-r_1)}{j - \frac{1}{2}}$$

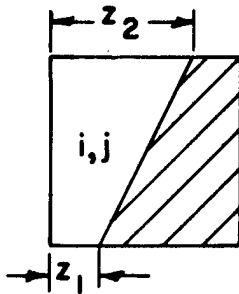
$$A_2 = 0$$

$$A_3 = \frac{\left(j - \frac{1-r_2}{2}\right)(1-r_2)}{j - \frac{1}{2}}$$

$$A_4 = 1$$

$$f_{i,j} = \frac{(J-1)(2-r_2-r_1) + 1 - r_1 r_2 - 1/3 (r_2-r_1)^2}{2j - 1}$$

3.



$$A_1 = 1$$

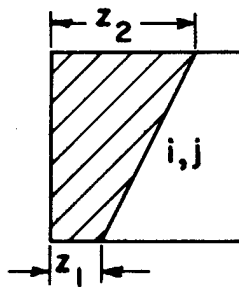
$$A_2 = z_1$$

$$A_3 = 0$$

$$A_4 = z_2$$

$$f_{i,j} = \frac{j z_2 + (j-1) z_1 - 1/3 (z_2-z_1)}{2j - 1}$$

4.



$$A_1 = 0$$

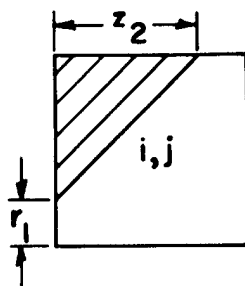
$$A_2 = 1 - z_1$$

$$A_3 = 1$$

$$A_4 = 1 - z_2$$

$$f_{i,j} = 1 - \frac{j z_2 + (j-1) z_1 - 1/3 (z_2 - z_1)}{2j - 1}$$

5.



$$A_1 = \frac{r_1(j - 1 + \frac{1}{2} r_1)}{j - \frac{1}{2}}$$

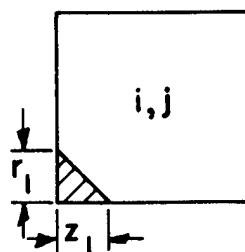
$$A_2 = 1$$

$$A_3 = 1$$

$$A_4 = 1 - z_2$$

$$f_{i,j} = 1 - \frac{z_2(1-r_1)[j - 1/3(1-r_1)]}{2j - 1}$$

6.



$$A_1 = \frac{(1-r_1)[j - \frac{1}{2}(1-r_1)]}{j - \frac{1}{2}}$$

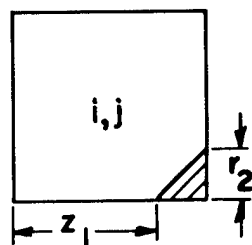
$$A_2 = 1 - z_1$$

$$A_3 = 1$$

$$A_4 = 1$$

$$f_{i,j} = 1 - \frac{z_1 r_1(j - 1 + 1/3 r_1)}{2j - 1}$$

7.



$$A_1 = 1$$

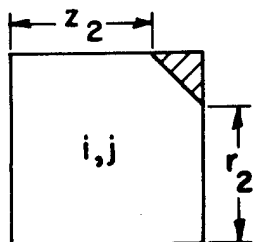
$$A_2 = z_1$$

$$A_3 = \frac{(1-r_2)[j - \frac{1}{2}(1-r_2)]}{j - \frac{1}{2}}$$

$$A_4 = 1$$

$$f_{i,j} = 1 - \frac{(1-z_1) r_2(j - 1 + 1/3 r_2)}{2j - 1}$$

8.



$$A_1 = 1$$

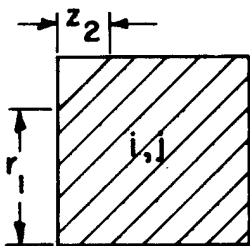
$$A_2 = 1$$

$$A_3 = \frac{r_2(j - 1 + \frac{1}{2} r_2)}{j - \frac{1}{2}}$$

$$A_4 = z_2$$

$$f_{i,j} = 1 - \frac{(1-z_2)(1-r_2)[j - 1/3(1-r_2)]}{2j - 1}$$

9.



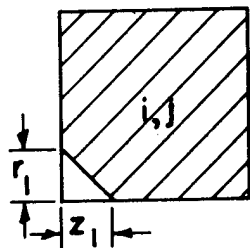
$$A_2 = 0$$

$$A_3 = 0$$

$$A_4 = z_2$$

$$f_{i,j} = \frac{z_2(1-r_1)[j - 1/3(1-r_1)]}{2j - 1}$$

10.



$$A_1 = \frac{r_1(j - 1 + \frac{1}{2} r_1)}{j - \frac{1}{2}}$$

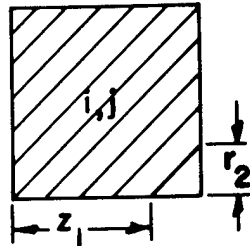
$$A_2 = z_1$$

$$A_3 = 0$$

$$A_4 = 0$$

$$f_{i,j} = \frac{z_1 r_1(j - 1 + 1/3 r_1)}{2j - 1}$$

11.



$$A_1 = 0$$

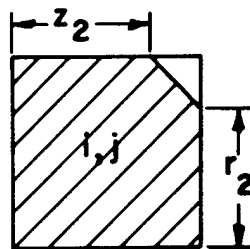
$$A_2 = 1 - z_1$$

$$A_3 = \frac{r_2(j - 1 + \frac{1}{2} r_2)}{j - \frac{1}{2}}$$

$$A_4 = 0$$

$$f_{i,j} = \frac{(1-z_1) r_2(j - 1 + 1/3 r_2)}{2j - 1}$$

12.



$$A_1 = 0$$

$$A_2 = 0$$

$$A_3 = \frac{(1-r_2) [j - \frac{1}{2} (1-r_2)]}{j - \frac{1}{2}}$$

$$A_4 = 1 - z_2$$

$$f_{i,j} = \frac{(1-z_2) (1-r_2) [j - 1/3 (1-r_2)]}{2j - 1}$$

APPENDIX III

The following six graphs show the changes in the Mach number of density in the region of the detached shock for the situations considered in this report. On each graph a series of plots are given for the appropriate quantity in different mesh rows. The position z equals zero represents the left-most extremity of the obstacle in the mesh. The estimated shock position is marked by an x on each plot and the approximate bounding region in which the shock front should lie is marked by small circles.

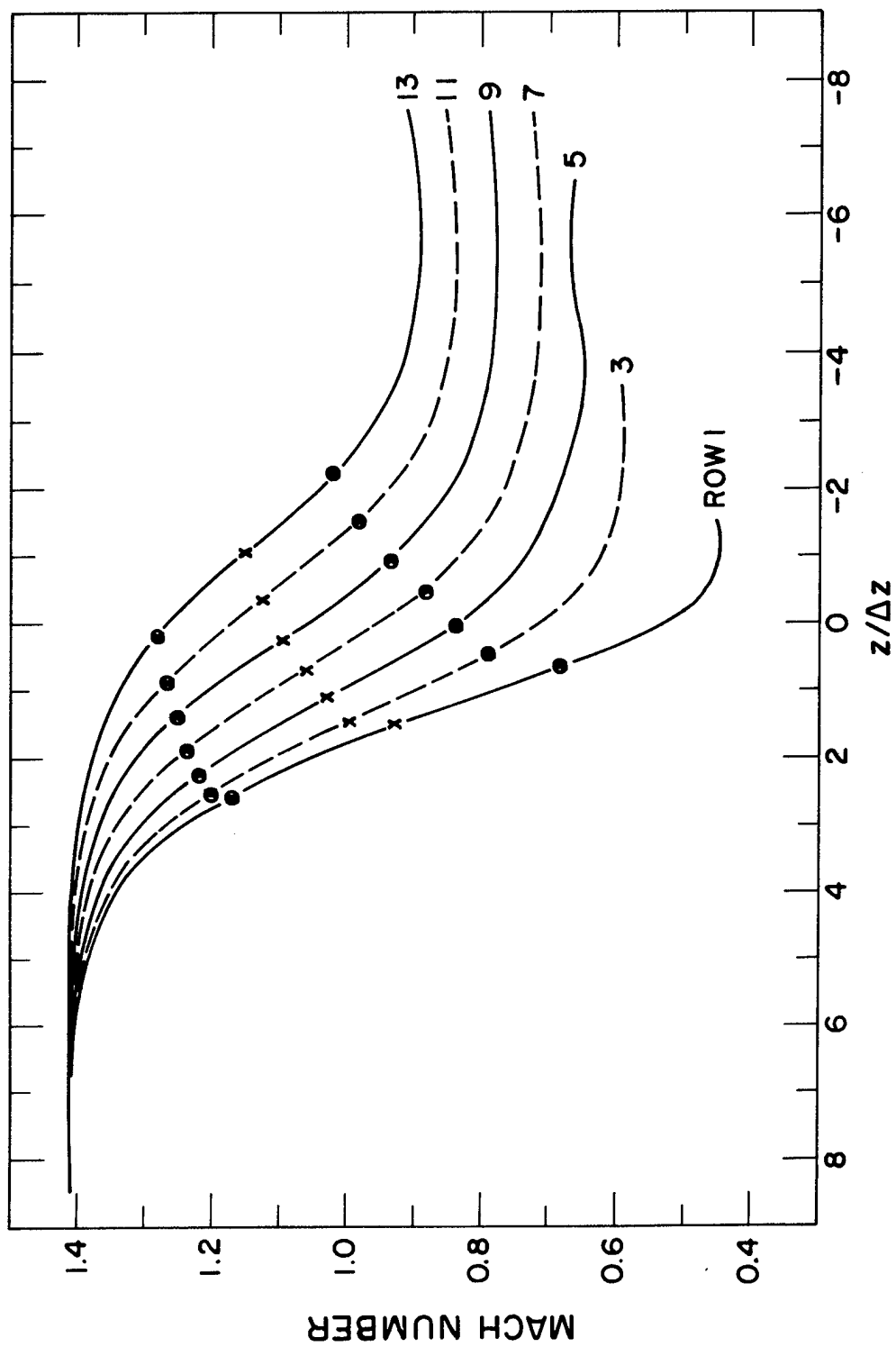


Figure III.1.1. 75° cone, Mach 1.41, 40 × 60 mesh

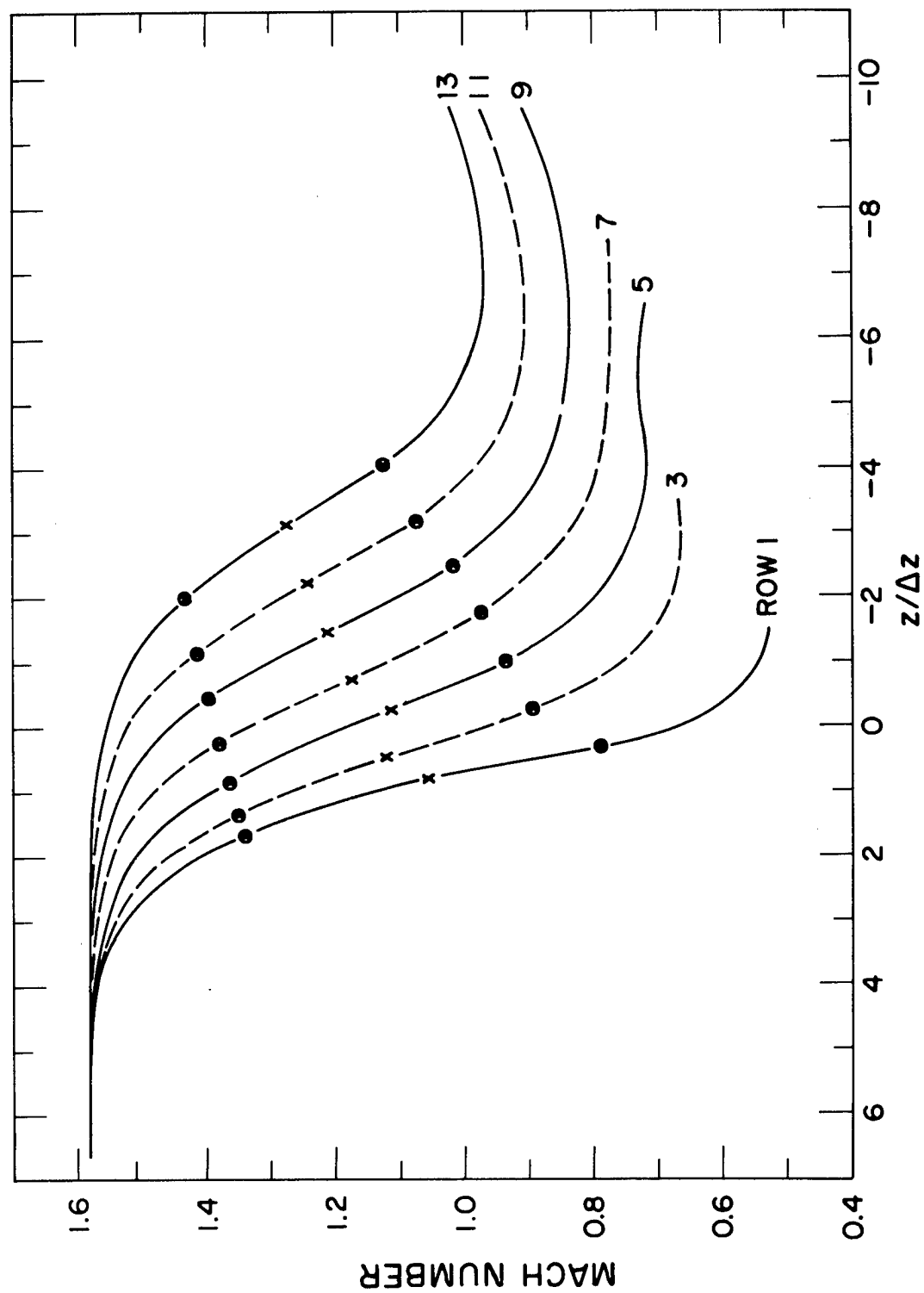


Figure III.2. 75° cone, Mach 1.58

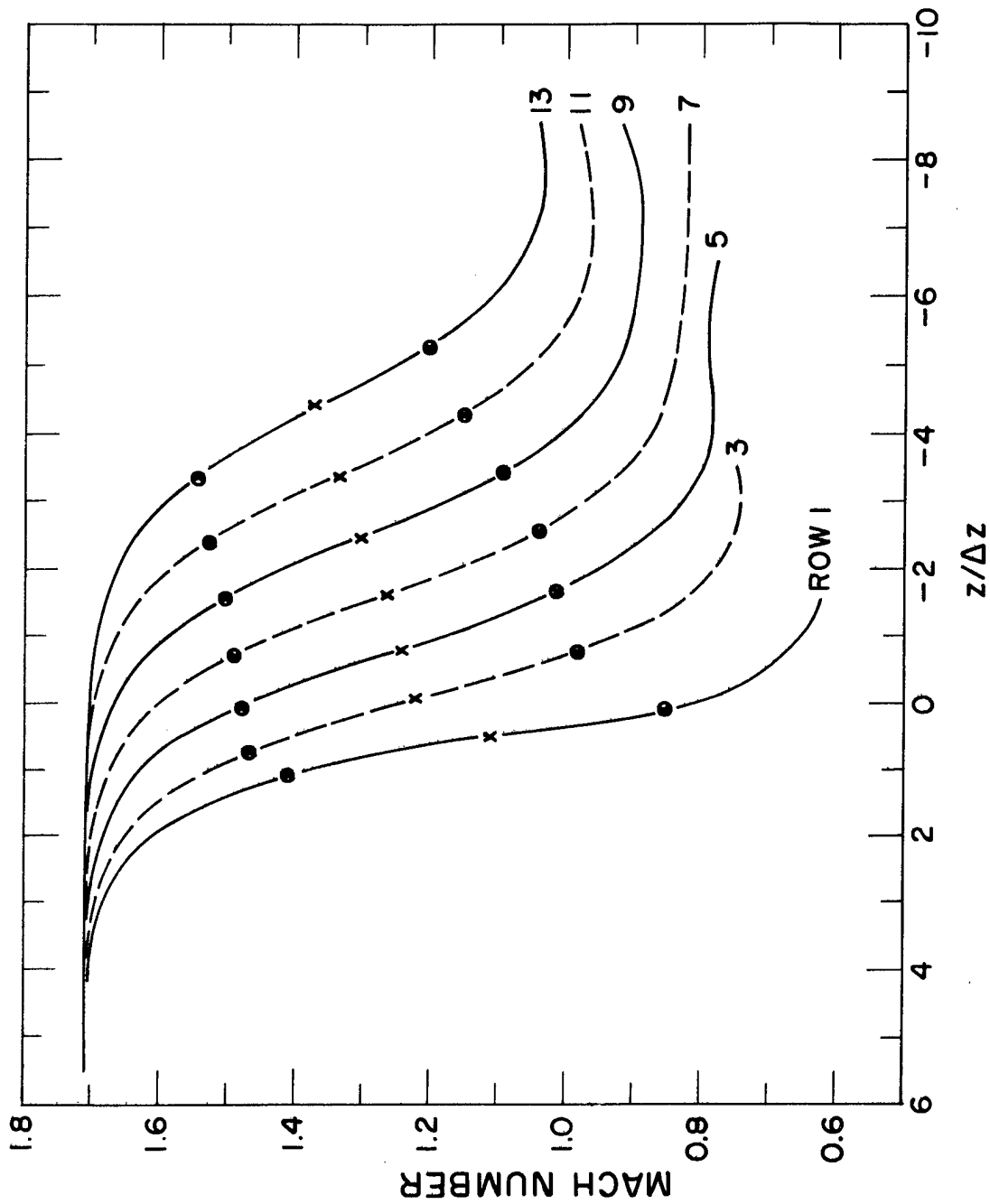


Figure III.3. 75° cone, Mach 1.71

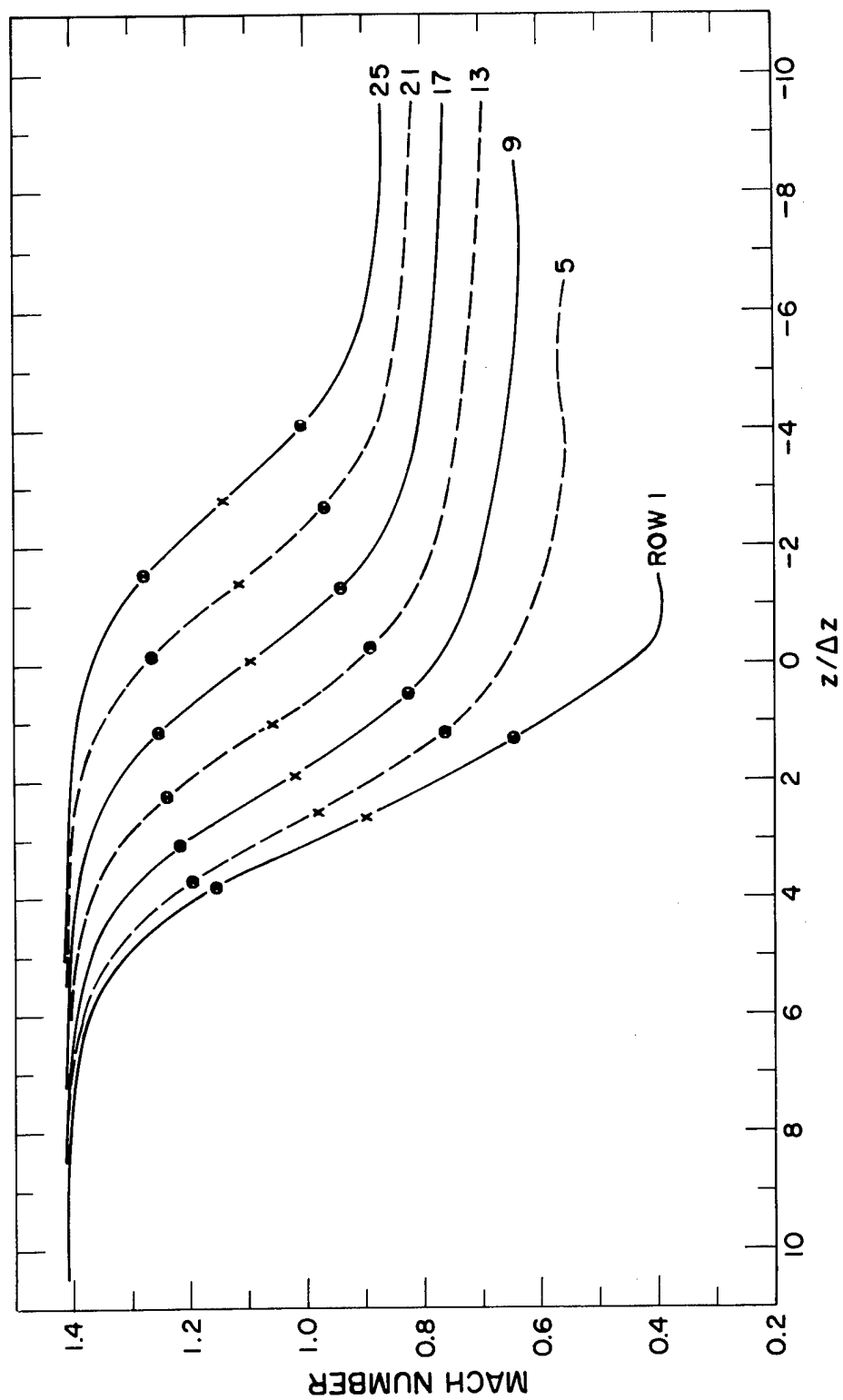


Figure III.4. 75° cone, Mach 1.41, 60×60 mesh

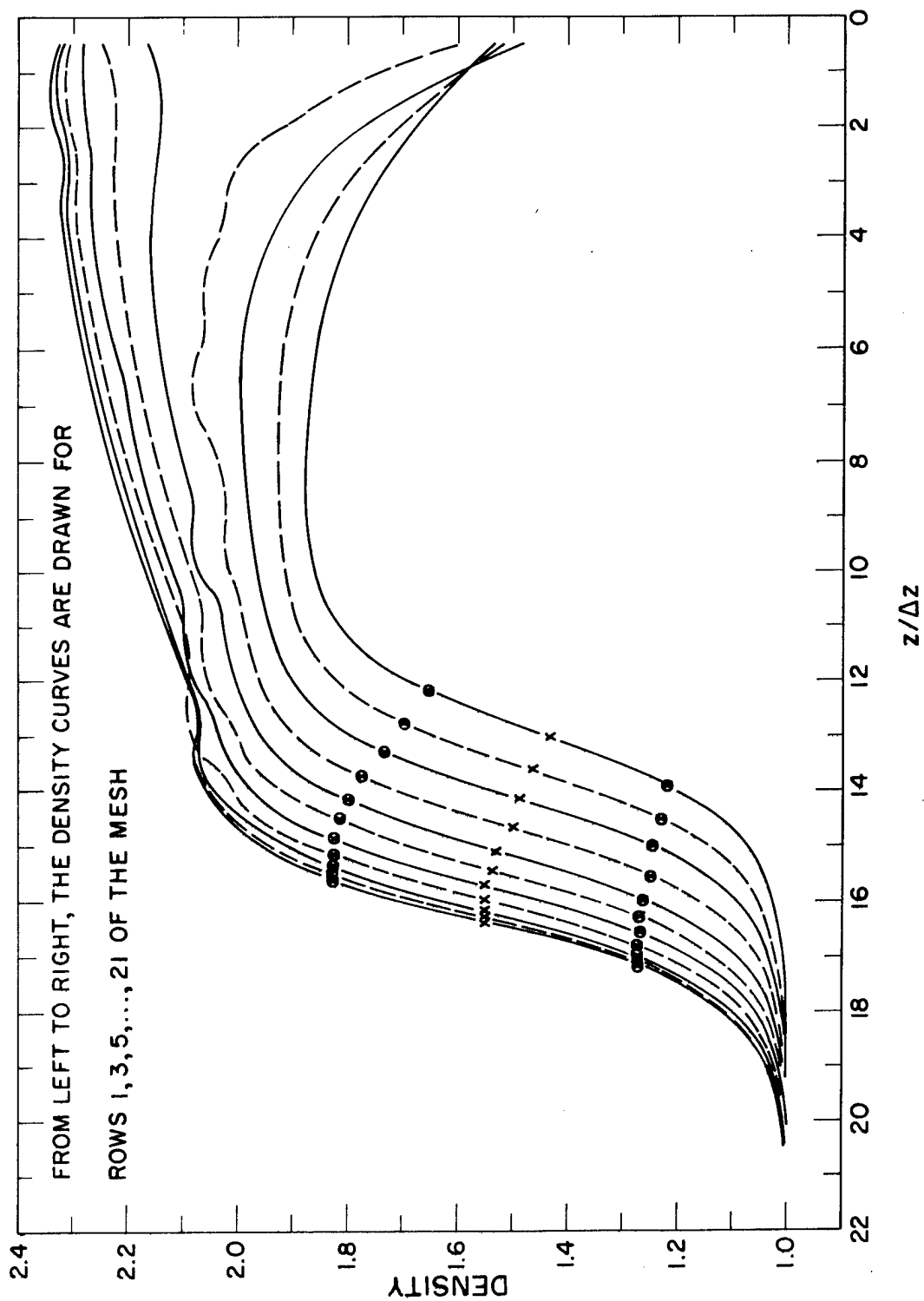


Figure III.5. 180° cone, Mach 1.58

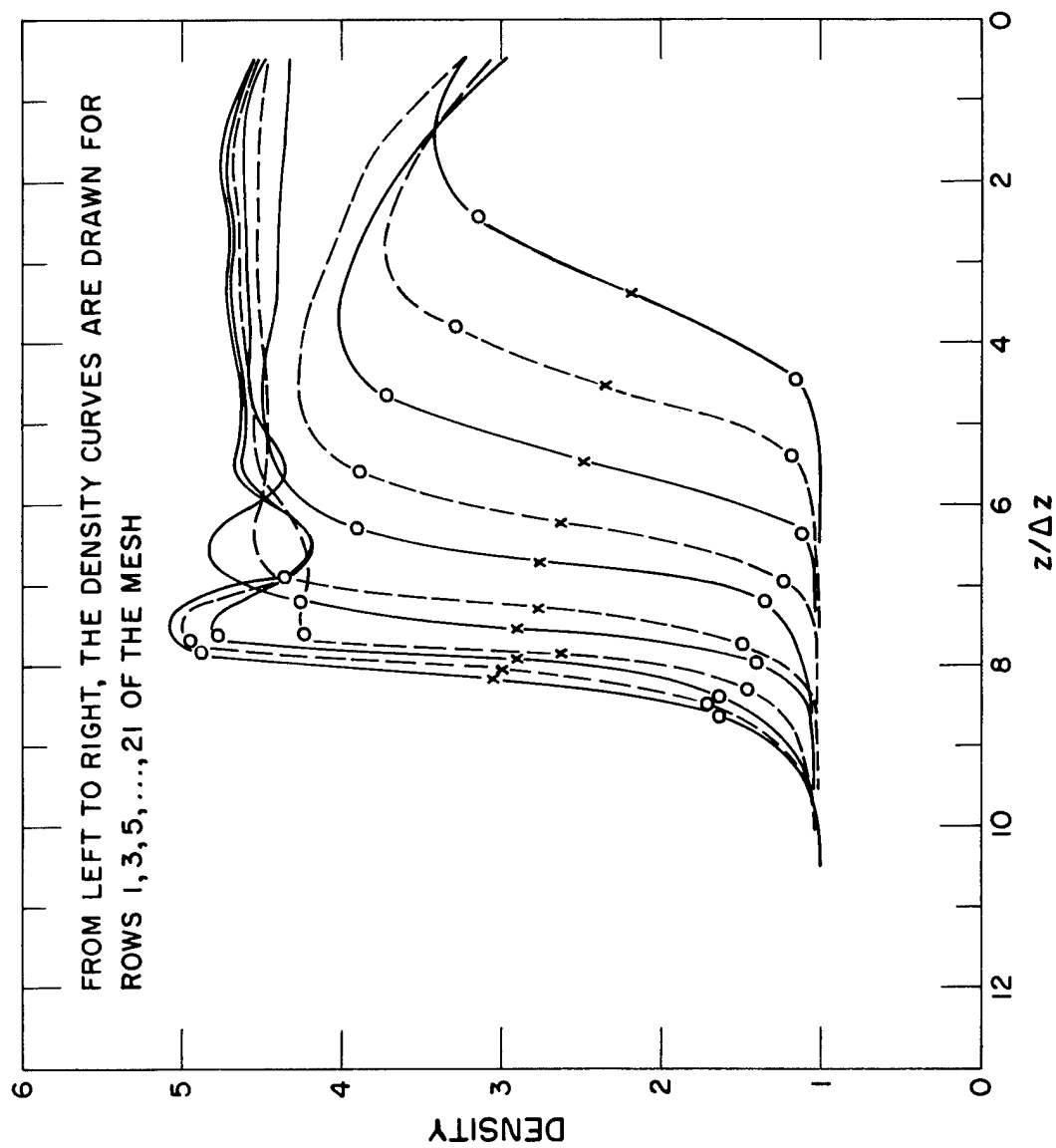


Figure III.6. 180° cone, Mach 4.3